AMP-activated protein kinase and adenylate kinase prevent ATP catastrophe and cytotoxic protein aggregation

Masak Takaine[1,2]*, Hiromi Imamura[3], Satoshi Yoshida[1,2,4,5]*

[1]Gunma University Initiative for Advanced Research (GIAR), Gunma University, Maebashi 371-8512, Japan

[2]Institute for Molecular and Cellular Regulation (IMCR), Gunma University, Maebashi 371-8512, Japan

[3]Graduate School of Biostudies, Kyoto University, Kyoto 606-8501, Japan

[4]School of International Liberal Studies, Waseda University, Tokyo, 169-8050, Japan

[5]Japan Science and Technology Agency, PREST

*Correspondence should be addressed to: masaktakaine@gunma-u.ac.jp (M.T.) (Lead contact) or satosh@waseda.jp (S.Y.)

Running title

ATP homeostasis prevents cytotoxic protein aggregation

Keywords

ATP, homeostasis, proteostasis, yeast, neurodegenerative disease, AMPK, protein aggregation

ABSTRACT

ATP is the major source of chemical energy in all life and maintained at several millimolar in eukaryotic cells. However, the underlying mechanism and physiological relevance of such high and stable concentrations of ATP remain unclear. Here we show that AMP-activated protein kinase (AMPK) and adenylate kinase (ADK) cooperate to maintain cellular ATP level regardless of glucose concentrations. Single cell imaging of ATP revealed that ATP concentrations in these mutants underwent stochastic and transient depletion of ATP repeatedly, inducing formation of cytotoxic aggregation of endogenous proteins and pathogenic proteins such as huntingtin and α-synuclein. Moreover, pharmacological elevation of ATP level in an ATP-reduced mutant prevented accumulation of α-synuclein aggregation and its cytotoxicity. Removal of the cytotoxic aggregates depends on proteasome, and proteasomal activity cooperates with AMPK or ADK to resist proteotoxic stresses. Our findings provided the first evidence that cellular ATP homeostasis ensures proteostasis and revealed that stochastic fluctuation of cellular ATP concentration could contribute for cytotoxic protein aggregation, implying that AMPK and ADK are important factors that prevent proteinopathy such as neurodegenerative diseases.

INTRODUCTION

Adenosine triphosphate (ATP) is a major energy currency used in all living organism. Due to its high demand, the turnover rate of ATP is estimated to be less than a minute in yeast and metazoans (Mortensen, Thaning et al., 2011, Takaine, Ueno et al., 2019). In addition to its role as energy currency, recent studies suggest ATP can influence the balance between soluble and aggregated states of proteins, suggesting proteostasis is maintained by energy dependent chaperones and by ATP's property as a hydrotrope to solubilize proteins (Hayes, Peuchen et al., 2018, Patel, Malinovska et al., 2017). Recent proteomics analysis has demonstrated that many cellular proteins are insoluble at submillimolar ATP concentration and become soluble at > 2 mM ATP concentrations (Sridharan, Kurzawa et al., 2019), although it is not known if the ATP-dependent protein solubilization/desolubilization has any significant roles in cell physiology.

Recently, we have established a reliable imaging technique to quantify intracellular ATP concentrations in single living yeast cells, using a genetically encoded fluorescent ATP biosensor QUEEN (Yaginuma, Kawai et al., 2014), enabling the evaluation of ATP homeostasis of individual cells for a long time period (Takaine et al., 2019). We have demonstrated that there is a little variation in intracellular ATP concentrations within a yeast population grown in the same culture (Takaine et al., 2019), contrasting with a large variation of intracellular ATP concentrations within a bacterial cell population (Yaginuma et al., 2014). Moreover, intracellular ATP concentrations in individual living yeast cells were stably and robustly maintained at around 4 mM, irrespective of carbon sources and cell cycle stages, and the temporal fluctuation of intracellular ATP concentration was quite small (Takaine et al., 2019). Based on the above observations, we hypothesized that there must exist an exceptionally robust mechanism to precisely regulate ATP concentrations in eukaryotes. We also wondered why ATP is stably maintained at high concentration far above the K_m (Michaelis constant) required for enzymatic activity of almost all the ATPases (Edelman, Blumenthal et al., 1987) and what consequence is associated with failure in ATP homeostasis in living organism.

The most promising candidate regulator for the ATP homeostasis is AMP-activated protein kinase (AMPK). AMPK, which is known to be activated by AMP and inhibited by ATP (Xiao, Heath et al., 2007), has been asserted for long periods of time as an important regulator for whole-body and cellular energy status in eukaryotes (Hardie, Schaffer et al., 2016). With increase in AMP: ATP or ADP: ATP ratio (*i.e.,* low-energy state), AMPK is activated and regulates its downstream effectors by phosphorylation to redirect the cell metabolism from

anabolic (ATP-consuming) state to catabolic (ATP-producing) state (Herzig & Shaw, 2017). In the budding yeast *Saccharomyces cerevisiae*, the sucrose non-fermenting 1 (Snf1) protein kinase complex corresponds to the sole AMPK. Like other AMPKs, yeast Snf1 complex comprises three subunits: the catalytic α subunit (*SNF1*), the scaffolding β subunit (*SIP1*, *SIP2* or *GAL83*) and the regulatory γ subunit (*SNF4*) (Ghillebert, Swinnen et al., 2011). The Snf1 complex has been well characterized for its role in adaptation to glucose limitation (Hedbacker & Carlson, 2008). In the presence of sufficient glucose in the medium, the Snf1 complex is inactive (Wilson, Hawley et al., 1996). When glucose concentration decreases, the Snf1 complex is activated and phosphorylates the transcriptional repressor Mig1, which then triggers transcription of numerous glucose-repressed genes (Carlson, 1999). However, contribution of AMPK or the Snf1 complex for cellular ATP level remains unknown.

Other possible candidate regulators for the ATP homeostasis include genes whose mutation leads to decrease in cellular content of ATP. Few yeast mutants, however, are known to have reduced ATP from biochemical analyses of the cell populations (Gauthier, Coulpier et al., 2008, Ljungdahl & Daignan-Fornier, 2012). Adenylate kinase (ADK) is a key enzyme that synthesizes ATP and AMP using two ADP molecules as substrates and null-mutant of ADK (*adk1*Δ) has reduced cellular ATP concentration (~70% of wild-type) (Gauthier et al., 2008). Bas1 is a transcription factor required for *de novo* purine synthesis and *bas1*Δ has also reduced ATP concentration (~50% of wild-type) (Gauthier et al., 2008). However, the regulation of ATP concentration and the physiological consequence of reduced ATP level in these mutants remain unaddressed, especially at single cell level.

In this study, we investigated the roles of the AMPK, ADK and Bas1 in ATP homeostasis using the QUEEN-based single cell ATP imaging technique. We demonstrated for the first time that AMPK is involved in regulation of intracellular ATP concentration even under glucose-rich conditions. In addition, time-lapse ATP imaging revealed that cells lacking both AMPK and ADK frequently underwent transient ATP depletion and those lacking Bas1 showed oscillation of ATP concentrations. Such ATP dynamics in the mutants have been overlooked in the previous biochemical studies. Interestingly, we found that some intrinsic proteins and aggregation-prone model proteins including α-synuclein, which is responsible for Parkinson's disease, aggregate and cause cytotoxicity in the all ATP-reduced mutants tested. Our findings suggest that stable maintenance of ATP is essential for proteostasis and imply that ATP crisis deteriorates proteinopathy such as neurodegenerative diseases.

RESULTS

AMPK is involved in maintenance of cellular ATP level

We have recently developed a reliable monitoring system for cytoplasmic ATP concentration in living yeast cells using an ATP biosensor QUEEN (Takaine et al., 2019). Taking advantage of this system, we conducted closer examination of ATP dynamics in wild-type and mutant yeast cells in this study. First, we tested whether deletion of *SNF1*, which encodes a catalytic subunit of AMPK, would affect cellular ATP concentration. In *SNF1*-null mutant (*snf1*Δ) cells, cellular ATP levels were significantly decreased compared to wild-type cells in all glucose concentrations tested (2%, 0.2%, 0.05%) (Fig 1A-B). It is of note that even under high-glucose conditions (2% glucose), where the Snf1 complex has been thought to be inactive, *snf1*Δ cells showed significantly reduced ATP levels. Moreover, deletion of each gene encoding β subunit of AMPK (*SIP1*, *SIP2* or *GAL83*) reduced cellular ATP level to a similar extent as deletion of *SNF1*, suggesting that three subtypes of the Snf1 complex are involved in maintaining ATP concentrations (Fig. 1C). On the other hand, deletion of *MIG1*, which encodes a major downstream target of the Snf1 complex in glucose repression, has little effect on ATP level (Fig. 1D), suggesting that unknown factors other than Mig1 primarily regulate ATP level under the control of the Snf1 complex. Taken together, these results demonstrate that AMPK/SNF1 affect cellular ATP concentrations even under glucose-rich conditions for the first time.

Adenylate kinase ADK1 cooperates with AMPK to regulate ATP homeostasis

Adenylate kinase catalyzes the interconversion of adenine nucleotides (ATP+AMP ⟷ 2ADP), which is important for *de novo* adenine nucleotide synthesis and for the balance of ATP, ADP and AMP. Indeed, previous biochemical studies reported that deletion of adenylate kinase gene reduced ATP concentrations in mouse skeletal muscle cells and budding yeasts (Gauthier et al., 2008, Janssen, Dzeja et al., 2000). We confirmed the results by using ATP imaging method: *adk1*Δ cells showed significantly lower QUEEN ratios compared to wild-type cells on average in the presence of sufficient carbon sources (Fig. S1).

In addition to being a key enzyme in purine metabolism, adenylate kinase also has been supposed to cooperate with AMPK to monitor cellular energy state (Hardie, Carling et al., 1998). We therefore compared ATP levels in *snf1*Δ *adk1*Δ double mutant cells with those in *snf1*Δ, *adk1*Δ and wild-type cells (Fig. 2A-B). The data were represented by a dot plot that can demonstrate the distribution characteristics in extensive details. *snf1Δ adk1Δ* cells showed a significant reduction in the average ATP level than the single mutant cells. Interestingly, we found not only a general reduction, but also a huge variation in the ATP level in *snf1*Δ, *adk1Δ,*

143 *snf1Δ adk1Δ* cell population as indicated by large value of coefficient of variance (CV) (Fig.
144 2B). Furthermore, there are some cells with extremely low ATP level in *snf1Δ adk1Δ* (Fig.
145 2A-B). These results suggest that both Adk1 and the Snf1 complex are synergistically
146 contributing for ATP homeostasis.
147

148 ## A large pool of adenine nucleotide is important for maintenance of cellular ATP
149 concentration

150 We also analysed a *bas1Δ* mutant, which is defective in expression of genes responsible for
151 adenine biogenesis (Daignan-Fornier & Fink, 1992, Denis, Boucherie et al., 1998). Consistent
152 with the previous biochemical data (Gauthier et al., 2008), ATP level quantified by QUEEN
153 was reduced by ~50 % in the *bas1Δ* cells (Fig. 2C-D). We found not only a general reduction,
154 but also a huge variation in the ATP level in *bas1Δ* cell population as indicated by large value of
155 CV (Fig. 2D). The reduction of ATP was indeed due to the reduced adenine biosynthesis
156 because feeding extra adenine in the media partially restored the ATP level (Fig. 2D). These
157 results suggest that sufficient production of adenine nucleotide is essential for stable
158 maintenance of ATP level. Moreover, the role of Bas1 in the ATP maintenance seemed to be
159 epistatic to that of Snf1 because *bas1Δ snf1Δ* double mutant cells showed a similar distribution
160 of ATP level as *bas1Δ* cells (Fig. S2).
161

162 ## ATP levels temporally fluctuate in the ATP mutant cells

163 To further explore the nature of large variation of ATP concentration in *snf1Δ adk1Δ* cells, we
164 employed time-lapse ATP imaging (Fig. 3). We observed that the QUEEN ratio often undergoes
165 a rapid decline followed by recovery in *snf1Δ adk1Δ* cells (see 116 min and 132 min in Fig. 3A
166 and C and movie S1, and 180 min and 356 min in Fig. 3B and D and movie S2). The sudden
167 drop in ATP concentration (hereafter called "ATP catastrophe") occurred within a few minutes
168 without any sign and was rarely observed in wild-type cells (Takaine et al., 2019). The ATP
169 catastrophe seemed to be a stochastic event and cell intrinsic: the events happened independent
170 of the cell cycle stages or cell size (compare Fig. 3C and D). In some occasion, the QUEEN
171 ratio did not recover after the ATP catastrophe and the cell died as judged by the loss of QUEEN
172 signals in the cell (Fig. S3). These observations suggest that the large variation of ATP
173 concentration in *snf1Δ adk1Δ* cells is not simply due to a mixed population with different basal
174 ATP levels, rather due to stochastic ATP catastrophe in individual cells.
175

176 Time-lapse imaging of *bas1Δ* revealed that there exists oscillatory cycles in the ATP
177 concentration (Figs. 3E and S4A, and movies S3 and S4): The ATP cycling in the *bas1Δ* was

178 slow (~35 min on average, Fig. S4B) and is distinguishable from that in the *snf1Δ adk1Δ*, but
179 the common characteristics of these mutants are that concentration of ATP reaches to near 0
180 mM repeatedly. ATP oscillation cycle was unsynchronized in the population and independent of
181 the cell cycle progression, suggesting that there exists unique metabolic rhythm intrinsic to
182 each cell. The oscillatory nature of ATP cycling in the *bas1Δ* mutant may involve
183 transcription/translation cycle and will be described elsewhere.
184
185 ATP homeostasis is required for preventing protein aggregation.
186 We have recently shown that cellular ATP concentration is stably maintained at ~4 mM in
187 budding yeast (Takaine et al., 2019) and demonstrated in this study that the Snf1/AMPK
188 complex, Adk1 and Bas1 are required for regulation of ATP homeostasis. However,
189 physiological importance of ATP homeostasis remains a question. To explore the significance
190 of high ATP concentration, we first examined global genetic interaction of *snf1Δ*, *adk1Δ*, and
191 *bas1Δ* using the CellMap ((Usaj, Tan et al., 2017), thecellmap.org). The *in silico* analysis
192 identified genes involved in "protein folding/glycosylation" as common negative genetic
193 interactors with *adk1Δ* and *bas1Δ* (Fig. 4A). Negative genetic interactors of *ura6*, a gene
194 encoding uridylate kinase that also has adenylate kinase activity, were also enriched in "protein
195 folding/glycosylation" category (Fig. 4A). We also found that interactors of *snf1* are implicated
196 in "protein folding/glycosylation". Interestingly, none of these mutants exhibit apparent genetic
197 interactions with genes in the "metabolism" category (Fig. 4A). The same analysis using
198 genetic and physical interactors provided similar results and showed many interactors were
199 enriched in "protein turnover" category (Fig. S5). These results imply that although these three
200 mutants regulate ATP in distinct mechanisms, all three have a common cellular function.
201
202 To examine possible defects in protein folding and turnover (*i.e.*, proteostasis), we challenged
203 these mutants with various proteotoxic stresses. We found little growth defects of ATP mutants
204 in a normal growth condition with 2% glucose at 30°C (control in Fig. 4B), suggesting that the
205 high concentration of ATP is not necessary for cellular growth. However, both *adk1* and *bas1*
206 mutants exhibited severe growth defects in high temperature at 40°C, 1 hour heat shock at 55°C,
207 0.5 μg/ml glycosylation inhibitor tunicamycin or 2 mM H_2O_2. *SNF1* deletion made the stress
208 sensitivity of *adk1Δ* further worse (Fig. 4B). The sensitivity to proteotoxic stress suggests that
209 ATP homeostasis mutants are defective in some aspects of proteostasis. We found that all four
210 mutants tested contained significantly increased number of Hsp104-GFP foci, a marker of
211 protein aggregation (Josefson, Andersson et al., 2017) (Fig. 4C-D). In contrast to Hsp104-GFP
212 foci, Pab1-GFP, a marker of stress granule (SG) assembly (Hoyle, Castelli et al., 2007) did not

form foci in the ATP mutants suggesting that protein aggregation and SG assembly are regulated in a distinct manner (Fig. 4D). These analyses identify abnormal protein aggregation as a common defect associated with ATP homeostasis mutants for the first time.

A transient depletion of ATP leads to formation of protein aggregation

To test if ATP depletion indeed triggers protein aggregation in living yeast, we artificially depleted cellular ATP by replacing glucose with 2-deoxyglucose (2DG), a strong inhibitor of glycolysis, in the media and monitored protein aggregation using Hsp104-GFP as a marker of protein aggregation (Josefson et al., 2017) in the wild-type cell. We have previously shown that ATP is almost completely depleted 2 minutes after 2DG treatment (Takaine et al., 2019). Within 15 min after 2DG treatment, more than 20% cells contained Hsp104-GFP foci indicative of protein aggregation (Fig. 5A-B). Importantly, unlike ATP, whose concentration recovers to the normal level within 1 min after glucose refeeding (Takaine et al., 2019), the dissolution kinetics of Hsp104-GFP was significantly slower (up to hours Fig. 5A-B).

To further confirm if high concentration of ATP is required for protein solubility, we also tested the Ubc9-ts protein, a model protein which is prone to aggregate (Kaganovich, Kopito et al., 2008) and found that ATP depletion by 2DG treatment triggered the Ubc9-ts protein aggregation (Fig. 5C). Thus, not only Hsp104-GFP positive intrinsic proteins but also extrinsic model proteins aggregate after ATP depletion.

It is known that stress granules (SG) are assembled in budding yeast cells after stressful conditions such as glucose depletion (Hoyle et al., 2007). In a sharp contrast to Hsp104-GFP foci formation, ATP depletion after 2DG treatment did not instantly trigger the formation of SG (Fig. S6). Consistent with the recent reports (Jain, Wheeler et al., 2016), our data suggest that SG formation requires ATP. We also note that Hsp104-GFP foci and SG did not co-localize, suggesting that these structures are derived from distinct mechanisms (Fig. S6). Thus, artificial depletion of ATP can trigger abnormal protein aggregation in living yeast cells.

ATP homeostasis is required for protection of cells from cytotoxicity caused by protein aggregation

Protein aggregation is often associated with neurodegenerative diseases such as Alzheimer's diseases, Huntington's diseases and Parkinson's diseases (Eftekharzadeh, Hyman et al., 2016). Mitochondrial failure has been also associated with many neurodegenerative diseases, but whether energy failure causes protein aggregation remained elusive as mitochondria also produce cytotoxic reactive oxygen species (ROS). (Bhat, Dar et al., 2015, Pathak, Berthet et al.,

248 2013). Abnormal aggregation of α-synuclein is known to be associated with Parkinson's
249 disease (Lashuel, Overk et al., 2013). To test if ATP is preventing formation of cytotoxic protein
250 aggregation, we examined the toxicity of α-synuclein-GFP (Syn-GFP) in budding yeast. As
251 previously shown, expression of Syn-GFP has little toxicity to wild-type yeast when expressed
252 under inducible *GAL1* promotor (Fig. 6A) (Outeiro & Lindquist, 2003, Sharma, Brandis et al.,
253 2006, Wijayanti, Watanabe et al., 2015). However, *snf1Δ, adk1Δ* and *bas1Δ* are hyper-sensitive
254 to the expression of Syn-GFP (Fig. 6A). We also found that *rpn4Δ*, which encodes a key
255 transcription factor for proteasomal subunits (Xie & Varshavsky, 2001), is very sensitive to the
256 Syn-GFP (Fig. 6A) consistent with the idea that Syn-GFP is degraded in ubiquitin-proteasomal
257 pathway in yeast (Tofaris, Kim et al., 2011, Wijayanti et al., 2015). Next we visualized the
258 cellular localization of Syn-GFP. As has been reported (Willingham, Outeiro et al., 2003),
259 Syn-GFP expressed in yeast is mainly localized to the plasma membrane (Fig. 6B-C). In
260 addition to the plasma membrane, we found Syn-GFP localized to punctated structures most
261 likely corresponding to protein aggregations (Fig.6B-C). Of note, the punctated structures are
262 not so obvious in *rpn4Δ* defective in proteasome, suggesting that the accumulation of Syn-GFP
263 puncta was not simply due to defective degradation.
264
265 To verify if high concentration of ATP protects cells from toxic protein aggregation, we
266 supplemented extra adenine to the medium (Fig. 6D). It has been shown that supplementing
267 300 μM adenine to the medium increases ATP concentration from 4 mM to 5.5 mM in
268 wild-type cell, 1 mM to 4 mM in *bas1Δ* cells (Gauthier et al., 2008) (similar results are shown
269 in Fig. 2D in this paper), and little or no change in *adk1Δ* from 2 mM to 2 mM (Gauthier et al.,
270 2008). Consistent with our hypothesis, addition of adenine reduced the Syn-GFP toxicity and
271 aggregation in *bas1Δ* but not *adk1Δ* (Fig. 6D). Thus, high concentration of ATP prevented
272 Syn-GFP aggregation and toxicity.
273
274 We also examined another model protein involved in neurodegenerative disease. PolyQ
275 containing Huntingtin protein tends to aggregate and is implicated in Huntington's disease
276 (Jiang, Poirier et al., 2005). We tested the toxicity of Htt103Q, a mutant form of huntingtin
277 protein which tends to aggregate and cause cytotoxicity in yeast (Meriin, Zhang et al., 2002).
278 Consistent with the idea that high concentration of ATP prevents protein aggregation, the ATP
279 homeostasis mutants *snf1Δ*, *adk1Δ*, *snf1Δ adk1Δ* and *bas1Δ* were very sensitive to Htt103Q
280 expression (Fig. S7).
281

282 Proteasome is essential for removal of protein aggregation caused by ATP depletion
283 Protein aggregation caused by ATP depletion was cytotoxic (Fig. 4B and Fig. 6A) and was not
284 easily dissolved after ATP repletion (Fig. 5). To seek for a pathway essential for removal of the
285 aggregates, we tested involvement of proteasome and autophagy.
286
287 Deletion of *RPN4*, which encodes a transcription factor of proteasomal genes (Xie &
288 Varshavsky, 2001), causes downregulation of proteasomal activity (Kruegel, Robison et al.,
289 2011) and showed synthetic growth defects with *adk1Δ*, *snf1Δ bas1Δ* at high temperature 38°C
290 and in the presence of H_2O_2 (Fig. 6E). In contrast to proteasome, autophagy did not have
291 apparent genetic interaction with above mutants (Fig. 6E). Deletion of essential component of
292 autophagic pathway *ATG1* did not affect the sensitivity of *adk1Δ*, *snf1Δ*, *bas1Δ* to high
293 temperature at 38°C or to the H_2O_2 (Fig. 6E). We also did not find accumulation Hsp104-GFP
294 foci in autophagy mutants *atg1*, *atg8* and *atg13* (not shown).
295
296 To test the involvement of proteasome in removal of protein aggregation after transient
297 depletion of ATP, we pretreated the cells with proteasomal inhibitor MG132 or DMSO and
298 analyzed a kinetics of Hsp104-GFP foci formation after 2DG treatment (Fig. 6F) using a
299 drug-sensitive yeast strain Y13206 (Piotrowski, Li et al., 2017). In both conditions, more than
300 90% cells exhibited Hsp104-GFP foci within 30 min of 2DG treatment. More than two-thirds of
301 the Hsp104-GFP foci was dissolved in the DMSO control while less than one-third was in the
302 MG132 treated samples indicating that proteasome is required for the dissolution process (Fig.
303 6F).

304 **DISCUSSION**

305 In this study, we have demonstrated for the first time that the Snf1 complex, budding yeast
306 AMPK, is required for the stable maintenance of cellular ATP concentration (ATP homeostasis)
307 in collaboration with adenylate kinase Adk1 (Fig. 7A). This function of the Snf1 complex in
308 ATP homeostasis is independent of glucose concentrations in the medium and is independent of
309 Mig1, the major transcriptional repressor involved in glucose repression (Fig. 1) and therefore
310 is distinct from its well-characterized role in adaptation to glucose limitation. Activity of the
311 Snf1 kinase complex might be sharply tuned depending on intracellular concentration of
312 adenine nucleotides or other metabolites indicative of cellular energy to prevent rapid ATP
313 catastrophe (Fig. 3) even in the presence of enough glucose. It is noteworthy that the reduction
314 of intracellular ATP concentration in *snf1Δ* cells in the presence of glucose have escaped
315 previous biochemical analysizes, again demonstrating the usefulness of the QUEEN-based ATP
316 imaging.
317
318 Since deletion of *BAS1* causes the most severe reduction of ATP level and is epistatic to *snf1Δ*,
319 a large pool size of adenine nucleotide is prerequisite for ATP homeostasis. This assumption is
320 reasonable because the pool size of recyclable ATP restricts ATP concentration given that the
321 rapid turnover rate of ATP. Bas1 would maintain the pool size of ATP by balancing ATP
322 synthesis and irreversible decreases such as incorporation into RNA and DNA (following
323 conversion to deoxy-ATP), degradation and excretion in rapidly proliferating yeasts.
324
325 We also have shown that key regulators of ATP homeostasis have roles in preventing cytotoxic
326 protein aggregation in budding yeast (Fig. 7B). The common feature associated with these
327 mutants are reduced level of ATP concentration, suggesting that high ATP level is essential for
328 protein solubilization.
329
330 Recent study has suggested that requirement of ATP may change depending on its
331 concentration. At low concentration below 0.5 mM, ATP mainly serves as a substrate for
332 enzymes such as protein kinases and heat shock protein chaperones, but at higher concentration
333 above 2 mM, ATP may have solubilizing effect on disordered proteins (Sridharan et al., 2019).
334 ATP homeostasis also might be required for constant driving proteasomal protein degradation
335 since it costs high amounts of ATP (Benaroudj, Zwickl et al., 2003, Tanaka, Waxman et al.,
336 1983).
337
338 Former biochemical measurements indicate that although ATP levels are reduced in *adk1* and

339 *bas1* mutants compared to wild-type, they still have ATP concentration above 2 mM (Gauthier
340 et al., 2008), which does not directly explain the accumulation of protein aggregations in these
341 mutants (Fig. 4) because most proteins are supposed to be soluble at > 2 mM ATP (Sridharan et
342 al., 2019). Visualization of ATP dynamics in living cells at single cell level revealed that ATP
343 undergoes transient depletion repeatedly (ATP catastrophe) in AMPK and ADK mutants
344 explaining how aggregation prone proteins aggregate and cause cytotoxicity. A similar, but
345 distinct instability of ATP was observed in *bas1Δ*, further confirming that ATP catastrophe
346 cause protein aggregation. Although the severe ATP depletion in these mutants are gradually
347 recovered by yet uncharacterized negative feedback regulation, the duration period of ~15 min
348 with reduced ATP can induce some proteins to form aggregates that last for generations.
349
350 Many neurodegenerative diseases such as Alzheimer's, Huntington's or Parkinson's are
351 associated with protein aggregation (Eisele, Monteiro et al., 2015, Josefson et al., 2017). On the
352 other hand, it has also been suggested that mitochondrial dysfunction and the accompanying
353 energy failure in nerve cells results in many types of neurodegenerative diseases based on a
354 body of evidence (Pathak et al., 2013). For example, there are reports showing that ATP level in
355 the brain is decreased in patients with early Parkinson's disease (Mochel, N'Guyen et al., 2012)
356 and that ATP synthesis in the brain is not properly regulated in patients with early Huntington's
357 disease (Hattingen, Magerkurth et al., 2009) and in the corresponding mouse model (Mochel,
358 Durant et al., 2012). Therefore, protein aggregation induced by ATP catastrophe revealed by
359 our study would link energy failure and protein aggregation, providing a comprehensive
360 insight into the onset of neurodegenerative diseases. It would be of great interest whether
361 ATP catastrophe is also taking place in neurons in potential patients of neurodegenerative
362 diseases or in the elderly. However, it seems to be obvious that neither biochemical
363 measurements nor mass spectrometry analysis is capable to detect ATP catastrophe because
364 of their insufficient time and space resolution. Thus, ATP imaging approach using the yeast
365 model system would be the first choice for examination of the molecular mechanism
366 underlying ATP homeostasis and ATP-catastrophe-induced protein aggregation.
367
368 A recent study reported that activation of AMPK by metformin ameliorates the progression of
369 Huntington's disease in a mouse model (Arnoux, Willam et al., 2018) and potential
370 therapeutic use of metformin for neurodegenerative disease is being discussed (Rotermund,
371 Machetanz et al., 2018). Also possible involvement of ATP and ADKs in preventing
372 manifestation of Parkinson's disease in mouse models and patients' are proposed
373 (Garcia-Esparcia, Hernandez-Ortega et al., 2015, Nakano, Imamura et al., 2017). Protein

374 aggregation induced by ATP catastrophe might be a general mechanism for development of
375 proteinopathy. Our study using ATP imaging reveals a physiological consequence of ATP
376 homeostasis failure in living cells for the first time and suggest that ATP homeostasis as a
377 promising target for preventing/treating neurodegenerative diseases.

378 **MATERIALS AND METHODS**

379 Yeast strains and plasmids

380 Budding yeast strains and plasmids used in this study are listed in Supplementary Tables S1 and
381 S2, respectively. These strains were constructed by a PCR-based method (Janke, Magiera et al.,
382 2004) and genetic crosses. The yeast knockout strain collection was originally purchased from
383 GE Healthcare (cat. # YSC1053).
384

385 Media, cell culture

386 Standard technic for yeast culture and manipulation was used (Guthrie & Fink, 2002). Synthetic
387 medium (SC) were prepared according to the recipe of Hanscho et al. (Hanscho, Ruckerbauer et
388 al., 2012). 2-Deoxy-D-glucose (2DG), tunicamycin and MG132 were purchased from
389 FUJIFILM Wako (cat. # 046-06483, 202-08241 and 139-18451, respectively). Tunicamycin
390 and MG132 were dissolved in dimethylsulfoxide (DMSO) to make stock solutions (5 mg/ml
391 and 42 mM, respectively). Cells were grown to mid-log phase at 30°C in the SC before imaging
392 unless otherwise noted.
393

394 Microscopy

395 Cells expressing Hsp104-GFP or GFP-Ubc9ts were concentrated by centrifugation and
396 sandwiched between a slide and a coverslip (No. 1.5 thickness, Matsunami, Osaka, Japan). The
397 immobilized cells were imaged using an inverted fluorescent microscope (Eclipse Ti-E, Nikon)
398 equipped with Apo TIRF 100× Oil DIC N2/NA 1.49 objective lens and an electron multiplying
399 charge-coupled device camera (iXon3 DU897E-CS0-#BV80, Andor) at around 25°C. The
400 Hsp104-GFP and GFP-Ubc9ts fluorescent signal was collected from stacks of 11 *z*-sections
401 spaced by 0.5 μm, and the maximum projections of the optical sections were shown in the Figs.
402 1-2, and S1. Cells expressing QUEEN were immobilized on a concanavalin A-coated
403 35-mm-glass bottom dish (#3971-035, No. 1.5 thickness, IWAKI). The dish was filled with
404 excess amount of medium (4.5–5 ml) against the cell volume to minimize changes in chemical
405 compositions of the medium during observation. The QUEEN fluorescence was acquired as
406 previously described (Takaine et al., 2019). Cells expressing α-synuclein-GFP were
407 immobilized on a slide glass as above, and the fluorescence signal was collected from a single
408 *z*-plane using an inverted fluorescent microscope (Eclipse Ti2-E, Nikon, Tokyo, Japan)
409 equipped with CFI Plan Apo λ 100× Oil DIC/NA1.45 objective lens and a CMOS image sensor

(DS-Qi2, Nikon). Images of cells were acquired from several fields of view for each experimental condition.

Data analysis

Numerical data were plotted using a KaleidaGraph software ver. 4.5.1 (Synergy Software). Means, SDs, and *p*-values were calculated using Excel software (Microsoft, WA, US). Significance between two sets of data was tested using an unpaired one-tailed Welch's *t*-test unless otherwise noted, and was indicated by an asterisk or by a *p*-value. The horizontal bar in dot plot indicates the average of each population. All the measurements were repeated at least twice to confirm the reproducibility.

Estimation of ATP concentration in yeast cells was carried out by using QUEEN-based ratiometric imaging as previously described (Takaine, 2019) (Takaine et al., 2019). The QUEEN ratio is proportional to ATP concentration and pseudo-colored to reflect its value throughout the paper. The mean QUEEN ratio inside of a cell represent the intracellular ATP concentration of the cell.

Autocorrelation functions (ACF) of the oscillation of QUEEN ratio were calculated using the R studio software ver. 3.4.1 (R Core Team, 2017). The apparent period of oscillation was estimated from the positive second peak of correlation coefficient, which was outside 95% confidence interval and statistically significant ($p < 0.05$), rejecting the assumption that there is no correlation.

ACKNOWLEDGEMENTS

We are grateful to the Yeast Genetic Resource Center, Y. Ohya, K. Ohashi, H. Takagi, D. Watanabe and J. Frydman for providing yeast strains and plasmids. We thank members of Yoshida/Takaine labs for their support. This work was supported by JSPS grants 16H04781 (S.Y. and M.T.), 15K18525 (M.T.) and Takeda Science foundation (S.Y.). This work was also supported by a joint research program of the Institute for Molecular and Cellular Regulation, Gunma University, Japan.

AUTHOR CONTRIBUTIONS

M.T. and S.Y. conceived and designed the project. M.T. conducted experiments and data analysis. H.I. provided a key reagent and expertise. M.T. and S.Y wrote the paper with inputs from H.I.

CONFLICT OF INTEREST

The authors declare no competing interests.

446 **REFERENCES**

447 Arnoux I, Willam M, Griesche N, Krummeich J, Watari H, Offermann N, Weber S, Narayan Dey P, Chen C,
448 Monteiro O, Buettner S, Meyer K, Bano D, Radyushkin K, Langston R, Lambert JJ, Wanker E, Methner A, Krauss
449 S, Schweiger S et al. (2018) Metformin reverses early cortical network dysfunction and behavior changes in
450 Huntington's disease. *Elife* 7

451 Baryshnikova A (2016) Systematic Functional Annotation and Visualization of Biological Networks. *Cell Syst*
452 2: 412-21

453 Benaroudj N, Zwickl P, Seemuller E, Baumeister W, Goldberg AL (2003) ATP hydrolysis by the proteasome
454 regulatory complex PAN serves multiple functions in protein degradation. *Mol Cell* 11: 69-78

455 Bhat AH, Dar KB, Anees S, Zargar MA, Masood A, Sofi MA, Ganie SA (2015) Oxidative stress,
456 mitochondrial dysfunction and neurodegenerative diseases; a mechanistic insight. *Biomed Pharmacother* 74:
457 101-10

458 Carlson M (1999) Glucose repression in yeast. *Curr Opin Microbiol* 2: 202-7

459 Cherry JM, Hong EL, Amundsen C, Balakrishnan R, Binkley G, Chan ET, Christie KR, Costanzo MC, Dwight
460 SS, Engel SR, Fisk DG, Hirschman JE, Hitz BC, Karra K, Krieger CJ, Miyasato SR, Nash RS, Park J, Skrzypek
461 MS, Simison M et al. (2012) Saccharomyces Genome Database: the genomics resource of budding yeast. *Nucleic*
462 *Acids Res* 40: D700-5

463 Daignan-Fornier B, Fink GR (1992) Coregulation of purine and histidine biosynthesis by the transcriptional
464 activators BAS1 and BAS2. *Proc Natl Acad Sci U S A* 89: 6746-50

465 Denis V, Boucherie H, Monribot C, Daignan-Fornier B (1998) Role of the myb-like protein bas1p in
466 Saccharomyces cerevisiae: a proteome analysis. *Mol Microbiol* 30: 557-66

467 Edelman AM, Blumenthal DK, Krebs EG (1987) Protein serine/threonine kinases. *Annu Rev Biochem* 56:
468 567-613

469 Eftekharzadeh B, Hyman BT, Wegmann S (2016) Structural studies on the mechanism of protein aggregation
470 in age related neurodegenerative diseases. *Mech Ageing Dev* 156: 1-13

471 Eisele YS, Monteiro C, Fearns C, Encalada SE, Wiseman RL, Powers ET, Kelly JW (2015) Targeting protein
472 aggregation for the treatment of degenerative diseases. *Nat Rev Drug Discov* 14: 759-80

473 Garcia-Esparcia P, Hernandez-Ortega K, Ansoleaga B, Carmona M, Ferrer I (2015) Purine metabolism gene
474 deregulation in Parkinson's disease. *Neuropathol Appl Neurobiol* 41: 926-40

475 Gauthier S, Coulpier F, Jourdren L, Merle M, Beck S, Konrad M, Daignan-Fornier B, Pinson B (2008)
476 Co-regulation of yeast purine and phosphate pathways in response to adenylic nucleotide variations. *Mol*
477 *Microbiol* 68: 1583-94

478 Ghillebert R, Swinnen E, Wen J, Vandesteene L, Ramon M, Norga K, Rolland F, Winderickx J (2011) The
479 AMPK/SNF1/SnRK1 fuel gauge and energy regulator: structure, function and regulation. *FEBS J* 278: 3978-90

480 Guthrie C, Fink GR (2002) *Guide to yeast genetics and molecular and cell Biology: Part C*. Gulf Professional

Publishing,

Hanscho M, Ruckerbauer DE, Chauhan N, Hofbauer HF, Krahulec S, Nidetzky B, Kohlwein SD, Zanghellini J, Natter K (2012) Nutritional requirements of the BY series of Saccharomyces cerevisiae strains for optimum growth. *FEMS Yeast Res* 12: 796-808

Hardie DG, Carling D, Carlson M (1998) The AMP-activated/SNF1 protein kinase subfamily: metabolic sensors of the eukaryotic cell? *Annu Rev Biochem* 67: 821-55

Hardie DG, Schaffer BE, Brunet A (2016) AMPK: An Energy-Sensing Pathway with Multiple Inputs and Outputs. *Trends Cell Biol* 26: 190-201

Hattingen E, Magerkurth J, Pilatus U, Mozer A, Seifried C, Steinmetz H, Zanella F, Hilker R (2009) Phosphorus and proton magnetic resonance spectroscopy demonstrates mitochondrial dysfunction in early and advanced Parkinson's disease. *Brain* 132: 3285-97

Hayes MH, Peuchen EH, Dovichi NJ, Weeks DL (2018) Dual roles for ATP in the regulation of phase separated protein aggregates in Xenopus oocyte nucleoli. *eLife* 7: e35224

Hedbacker K, Carlson M (2008) SNF1/AMPK pathways in yeast. *Front Biosci* 13: 2408-20

Herzig S, Shaw RJ (2017) AMPK: guardian of metabolism and mitochondrial homeostasis. *Nat Rev Mol Cell Biol* 19: 121

Hoyle NP, Castelli LM, Campbell SG, Holmes LE, Ashe MP (2007) Stress-dependent relocalization of translationally primed mRNPs to cytoplasmic granules that are kinetically and spatially distinct from P-bodies. *J Cell Biol* 179: 65-74

Jain S, Wheeler JR, Walters RW, Agrawal A, Barsic A, Parker R (2016) ATPase-Modulated Stress Granules Contain a Diverse Proteome and Substructure. *Cell* 164: 487-98

Janke C, Magiera MM, Rathfelder N, Taxis C, Reber S, Maekawa H, Moreno-Borchart A, Doenges G, Schwob E, Schiebel E, Knop M (2004) A versatile toolbox for PCR-based tagging of yeast genes: new fluorescent proteins, more markers and promoter substitution cassettes. *Yeast* 21: 947-62

Janssen E, Dzeja PP, Oerlemans F, Simonetti AW, Heerschap A, de Haan A, Rush PS, Terjung RR, Wieringa B, Terzic A (2000) Adenylate kinase 1 gene deletion disrupts muscle energetic economy despite metabolic rearrangement. *EMBO J* 19: 6371-81

Jiang H, Poirier MA, Ross CA (2005) A structure-based analysis of huntingtin mutant polyglutamine aggregation and toxicity: evidence for a compact beta-sheet structure. *Hum Mol Genet* 14: 765-774

Josefson R, Andersson R, Nyström T (2017) How and why do toxic conformers of aberrant proteins accumulate during ageing? *Essays Biochem* 61: 317

Kaganovich D, Kopito R, Frydman J (2008) Misfolded proteins partition between two distinct quality control compartments. *Nature* 454: 1088-95

Kruegel U, Robison B, Dange T, Kahlert G, Delaney JR, Kotireddy S, Tsuchiya M, Tsuchiyama S, Murakami CJ, Schleit J, Sutphin G, Carr D, Tar K, Dittmar G, Kaeberlein M, Kennedy BK, Schmidt M (2011) Elevated

516 proteasome capacity extends replicative lifespan in Saccharomyces cerevisiae. *PLoS Genet* 7: e1002253
517 Lashuel HA, Overk CR, Oueslati A, Masliah E (2013) The many faces of alpha-synuclein: from structure and
518 toxicity to therapeutic target. *Nat Rev Neurosci* 14: 38-48
519 Ljungdahl PO, Daignan-Fornier B (2012) Regulation of amino acid, nucleotide, and phosphate metabolism in
520 Saccharomyces cerevisiae. *Genetics* 190: 885-929
521 Meriin AB, Zhang X, He X, Newnam GP, Chernoff YO, Sherman MY (2002) Huntington toxicity in yeast
522 model depends on polyglutamine aggregation mediated by a prion-like protein Rnq1. *J Cell Biol* 157: 997-1004
523 Mochel F, Durant B, Meng X, O'Callaghan J, Yu H, Brouillet E, Wheeler VC, Humbert S, Schiffmann R, Durr
524 A (2012) Early alterations of brain cellular energy homeostasis in Huntington disease models. *J Biol Chem* 287:
525 1361-70
526 Mochel F, N'Guyen TM, Deelchand D, Rinaldi D, Valabregue R, Wary C, Carlier PG, Durr A, Henry PG
527 (2012) Abnormal response to cortical activation in early stages of Huntington disease. *Mov Disord* 27: 907-10
528 Mortensen SP, Thaning P, Nyberg M, Saltin B, Hellsten Y (2011) Local release of ATP into the arterial inflow
529 and venous drainage of human skeletal muscle: insight from ATP determination with the intravascular
530 microdialysis technique. *The Journal of Physiology* 589: 1847-1857
531 Nakano M, Imamura H, Sasaoka N, Yamamoto M, Uemura N, Shudo T, Fuchigami T, Takahashi R, Kakizuka
532 A (2017) ATP Maintenance via Two Types of ATP Regulators Mitigates Pathological Phenotypes in Mouse
533 Models of Parkinson's Disease. *EBioMedicine* 22: 225-241
534 Outeiro TF, Lindquist S (2003) Yeast cells provide insight into alpha-synuclein biology and pathobiology.
535 *Science* 302: 1772-5
536 Patel A, Malinovska L, Saha S, Wang J, Alberti S, Krishnan Y, Hyman AA (2017) ATP as a biological
537 hydrotrope. *Science* 356: 753-756
538 Pathak D, Berthet A, Nakamura K (2013) Energy failure: does it contribute to neurodegeneration? *Ann Neurol*
539 74: 506-16
540 Piotrowski JS, Li SC, Deshpande R, Simpkins SW, Nelson J, Yashiroda Y, Barber JM, Safizadeh H, Wilson E,
541 Okada H, Gebre AA, Kubo K, Torres NP, LeBlanc MA, Andrusiak K, Okamoto R, Yoshimura M, DeRango-Adem
542 E, van Leeuwen J, Shirahige K et al. (2017) Functional annotation of chemical libraries across diverse biological
543 processes. *Nature Chemical Biology* 13: 982
544 R Core Team (2017) R: A Language and Environment for Statistical Computing. In Vienna, Austria: R
545 Foundation for Statistical Computing
546 Rotermund C, Machetanz G, Fitzgerald JC (2018) The Therapeutic Potential of Metformin in
547 Neurodegenerative Diseases. *Front Endocrinol (Lausanne)* 9: 400
548 Sharma N, Brandis KA, Herrera SK, Johnson BE, Vaidya T, Shrestha R, DebBurman SK (2006) α-synuclein
549 budding yeast model. *J Mol Neurosci* 28: 161-178
550 Sridharan S, Kurzawa N, Werner T, Günthner I, Helm D, Huber W, Bantscheff M, Savitski MM (2019)

Proteome-wide solubility and thermal stability profiling reveals distinct regulatory roles for ATP. *Nature Communications* 10: 1155

Takaine M (2019) QUEEN-based Spatiotemporal ATP Imaging in Budding and Fission Yeast. *Bio-protocol* 9: e3320

Takaine M, Ueno M, Kitamura K, Imamura H, Yoshida S (2019) Reliable imaging of ATP in living budding and fission yeast. *J Cell Sci* 132

Tanaka K, Waxman L, Goldberg AL (1983) ATP serves two distinct roles in protein degradation in reticulocytes, one requiring and one independent of ubiquitin. *J Cell Biol* 96: 1580-5

Tofaris GK, Kim HT, Hourez R, Jung JW, Kim KP, Goldberg AL (2011) Ubiquitin ligase Nedd4 promotes alpha-synuclein degradation by the endosomal-lysosomal pathway. *Proc Natl Acad Sci U S A* 108: 17004-9

Usaj M, Tan Y, Wang W, VanderSluis B, Zou A, Myers CL, Costanzo M, Andrews B, Boone C (2017) TheCellMap.org: A Web-Accessible Database for Visualizing and Mining the Global Yeast Genetic Interaction Network. *G3 (Bethesda)* 7: 1539-1549

Wijayanti I, Watanabe D, Oshiro S, Takagi H (2015) Isolation and functional analysis of yeast ubiquitin ligase Rsp5 variants that alleviate the toxicity of human α-synuclein. *The Journal of Biochemistry* 157: 251-260

Willingham S, Outeiro TF, DeVit MJ, Lindquist SL, Muchowski PJ (2003) Yeast genes that enhance the toxicity of a mutant huntingtin fragment or alpha-synuclein. *Science* 302: 1769-72

Wilson WA, Hawley SA, Hardie DG (1996) Glucose repression/derepression in budding yeast: SNF1 protein kinase is activated by phosphorylation under derepressing conditions, and this correlates with a high AMP:ATP ratio. *Curr Biol* 6: 1426-34

Xiao B, Heath R, Saiu P, Leiper FC, Leone P, Jing C, Walker PA, Haire L, Eccleston JF, Davis CT, Martin SR, Carling D, Gamblin SJ (2007) Structural basis for AMP binding to mammalian AMP-activated protein kinase. *Nature* 449: 496-500

Xie Y, Varshavsky A (2001) RPN4 is a ligand, substrate, and transcriptional regulator of the 26S proteasome: a negative feedback circuit. *Proc Natl Acad Sci U S A* 98: 3056-61

Yaginuma H, Kawai S, Tabata KV, Tomiyama K, Kakizuka A, Komatsuzaki T, Noji H, Imamura H (2014) Diversity in ATP concentrations in a single bacterial cell population revealed by quantitative single-cell imaging. *Sci Rep* 4: 6522

580 **FIGURE LEGENDS**

581 Fig. 1. AMPK is involved in maintenance of cellular ATP level in non-starving cells

582 (A) Visualization of intracellular ATP levels in wild-type (WT) and *snf1Δ* cells by using the
583 ATP sensor QUEEN. Cells were grown to mid-log phase in SC-H medium containing the
584 indicated concentrations of glucose and then imaged. White scale bar = 5 μm. (B) *snf1Δ* cells
585 showed reduced ATP levels compared to wild-type cells. The mean QUEEN ratio inside a
586 single cell (mean QUEEN ratio/cell), which represents intracellular ATP level of the cell, was
587 quantified for each cell from the ratio image. Data are the mean of the cell population ± 1SD
588 (error bar) normalized to the wild-type. N = 105–193 cells were scored. Asterisks indicate
589 statistical significance against WT ($p < 0.05$). (C) ATP levels in single-deletion mutants of
590 AMPK *β* subunits. Data are the mean of the cell population ± 1SD (error bar) normalized to
591 the wild-type. N = 177–223 cells were scored. Asterisks indicate statistical significance
592 between the two strains (*, $p < 0.05$; **, $p < 0.01$). N.S., no significance. (D) *mig1Δ* cells
593 showed slightly reduced ATP levels compared to wild-type cells. Data are the mean of the cell
594 population ± 1SD (error bar) normalized to the wild-type. N = 190–231 cells were scored.
595 Asterisks indicate statistical significance between the two strains.

596

597 Fig. 2 Both interconversion and active synthesis of adenine nucleotides are also
598 important for ATP homeostasis

599 (A) Adk1 and Snf1 synergistically control cellular ATP levels. QUEEN ratio images of the ATP
600 homeostasis mutants cells grown in the medium containing 2% glucose. An asterisk indicates
601 an example of cells with significantly reduced ATP level. (B) Mean QUEEN ratios of cells were
602 translated to the ATP concentration and shown in a dot plot. The horizontal bar indicates the
603 mean of each population. Asterisks indicate *p*-values versus WT: *=1.5×10^{-59}, **=2.3×10^{-34},
604 ***=2.9×10^{-117}. CV: coefficient of variance. N = 134–276 cells were scored. (C) QUEEN ratio
605 images of *bas1Δ* cells grown in the 2% glucose medium. Growth in the media supplemented
606 with 0.11 mg/ml adenine partially restored the low ATP phenotype of the *bas1*Δ. (D) The ATP
607 concentrations of the cells shown in (C) were plotted. Asterisks indicate *p*-values: *=2.3×10^{-160},
608 **=8.8×10^{-12} (versus WT in glucose), ***=3.6×10^{-20} (versus *bas1*Δ in glucose). CV:
609 coefficient of variance. N = 186–296 cells were scored.

610

611 Fig. 3 Temporal fluctuation of ATP levels in *snf1*Δ*adk1*Δ and *bas1*Δ cells

612 (A, C) Time-lapse imaging of the QUEEN in *snf1*Δ *adk1*Δ cells in the 2% glucose medium.
613 Images at the representative time points were shown. The QUEEN ratio was dropped twice
614 (indicated by arrowheads) with short interval. See also movie S1. Data were converted into ATP

615 concentrations and plotted in (C). (B, D) Another example of time-lapse imaging of the
616 QUEEN in *snf1*Δ*adk1*Δ cells in the 2% glucose medium. The QUEEN ratio was dropped twice
617 (indicated by arrowheads) with long interval. See also movie S2. Data were converted into ATP
618 concentrations and plotted in (D). (E) A time-lapse imaging of the QUEEN in *bas1*Δ in the 2%
619 glucose medium. The ATP concentration of the mother (cell-1) and the daughter (cell-2) were
620 plotted in the bottom. Images at the representative time points were shown on the top. Note that
621 the QUEEN ratio is synchronized until the cells undergo cell separation at the time point 76 min
622 indicated by an arrow. After separation, each cell has unique periodic cycle of the ATP. The
623 movie is available in the movie S3. White scale bar = 5 μm.
624
625 Fig. 4. ATP homeostasis is required for preventing protein aggregation
626 (A) Functional landscape of the known interactors of ATP mutants. Negative genetic interactors
627 of the indicated gene were derived from SGD database (https://www.yeastgenome.org/)
628 (Cherry, Hong et al., 2012) and overlaid on a functional map based on the global genetic
629 interaction network of the yeast genome (Baryshnikova, 2016, Usaj et al., 2017). *URA6*
630 encodes an uridylate kinase essential for viability, which also have adenylate kinase activity.
631 (B) Each strain of indicated genotype was serially diluted (five-fold) and spotted on the SC +
632 2% glucose medium and grown in the indicated stress conditions. Photos were taken after 2-3
633 days. (C) Formation of Hsp104-GFP foci in ATP homeostasis mutants. GFP signal (inverted
634 grayscale) was imaged in the log phase culture of the indicated mutant cells expressing
635 Hsp104-GFP at 35°C. (D) Quantification of the data shown in (C). Data from similar
636 experiments using strains expressing Pab1-GFP, instead of Hsp104-GFP, were also plotted.
637 Values are the mean ± 1SD (error bars). Asterisks indicate statistical significance against WT (p
638 < 0.05) (N=3–4). White scale bar = 5 μm.
639
640 Fig. 5 ATP depletion triggers protein aggregation in living yeast cells
641 (A) Hsp104-GFP foci formation after ATP depletion. Wild type cells expressing Hsp104-GFP
642 were grown to log phase at 35°C in the medium containing 2% glucose. At the time point 0 min,
643 the medium was replaced with 20 mM 2DG (red) or 2% glucose (as a control; blue). The cells
644 were released back to the media containing 2% glucose at the time point 50 min. Cells were
645 imaged at the indicated time-points, classified and scored according to the number of
646 Hsp104-GFP foci. Values are the mean (N = 3). Asterisks indicate statistical significance
647 against 2% glucose treatment ($p < 0.05$). (B) Representative images of cells analyzed in (A).
648 (C) Formation of Ubc9-ts foci after ATP depletion. Cells expressing GFP-Ubc9-ts under an
649 inducible *GAL* promoter were grown in the medium containing 2% galactose (SC-gal) at 33°C,

650 and then the medium was exchanged with 2DG or SC-gal. After 30 min, cells were imaged and
651 scored for the number of GFP-Ubc9-ts foci. Representative images (inverted grayscale) are
652 shown in the left and summarized in the right. Values are the mean ± 1SD (error bars) (N = 4).
653 White scale bar = 5 μm.
654
655 Fig. 6 Aggregation and cytotoxicity of α-synuclein depends on ATP homeostasis
656 (A) Each strain of indicated genotype was transformed with an expression vector carrying
657 α-synuclein-GFP or GFP, serially diluted (five-fold) and spotted on SC + 2% galactose plate,
658 and then grown for 3 days at 30°C. (B) Localization of α-synuclein-GFP in ATP mutants. Cells
659 were grown on galactose plates for more than 42 h at 30°C, and then imaged. Representative
660 images of α-synuclein-GFP (inverted grayscale) are shown. (C) Quantification of the data
661 shown in (B). Cells were classified and scored for the localization pattern of α-synuclein-GFP.
662 Percent of cells showing α-synuclein-GFP foci are plotted. Data are the mean ± 1SD (error
663 bars) from 3–6 independent observations. N = 33–380 cells were scored in each measurement.
664 *P*-values versus WT are shown. N.S., no significance (*p*-value > 0.05). (D) *(top)* Each strain of
665 indicated genotype was transformed with an expression vector carrying α-synuclein-GFP and
666 grown on galactose plates containing 0 mM (− Adenine) or 0.3 mM (+ Adenine) adenine for 3
667 days at 30°C. *(bottom)* Cells were grown on galactose plates in the absence or presence of
668 adenine for 41-45 h at 30°C, and then imaged. Percent of cells showing α-synuclein-GFP foci
669 are plotted. Data are the mean ± 1SD (error bars) from 5 independent transformants. N = 53–
670 258 cells were scored in each measurement. *P*-values versus "– Adenine" are shown. (E) Each
671 strain of indicated genotype was serially diluted (five-fold) and spotted on the SC + 2% glucose
672 medium and grown in the indicated stress conditions. (F) Cells of a drug-sensitive strain
673 Y13206 were grown to log phase at 37°C in the medium containing 2% glucose and
674 supplemented with 0.1% DMSO or 0.1% DMSO plus 42 μM MG132 at $t = -30$ min. At $t = 0$
675 min, these cells were washed and released in the medium containing 20 mM 2DG ± MG132,
676 and then the cells were washed and released again in the medium containing 2% glucose ±
677 MG132. Cells were imaged at indicated time points and scored for the number of Hsp104-GFP
678 foci. Data are the mean ± 1SD (error bars). Asterisks indicate statistical significance against
679 DMSO ($p < 0.02$) (N=3).
680
681 Fig. 7 Models for ATP homeostasis and its role for proteostasis
682 (A) Schematic summary of the roles of Snf1, Adk1, and Bas1 in ATP homeostasis. (B) A
683 schematic model for ATP homeostasis preventing cytotoxic protein aggregation.
684

685 **SUPPLEMENTARY INFORMATION**

686 Supplementary figure legends

687 Fig. S1 Adenylate kinase Adk1 is involved in maintenance of cellular ATP
688 concentration

689 (A) QUEEN ratio images of wild-type and *adk1Δ* cells grown in 2% glucose or 2% galactose.
690 White scale bar = 5 μm. (B) Quantification of data shown in (A). Mean QUEEN ratio/cell was
691 quantified for each cell from the ratio images. Values are the mean of the cell population ± 1SD
692 (error bar). N = 182–236 cells were scored. Asterisks indicate statistical significance against
693 WT ($p < 0.05$).

694

695 Fig. S2 ATP levels in *bas1*Δ *snf1*Δ cells

696 (A) QUEEN ratio images of wild-type, *bas1Δ*, *snf1Δ* and *bas1Δ snf1Δ* cells. (B) Quantification
697 of data shown in (A). Mean QUEEN ratio/cell was quantified for each cell from the ratio
698 images. Data are shown as a dot plot. The horizontal bar in the plot indicates the mean of each
699 population. Significance between two sets of data was tested using an unpaired two-tailed
700 Welch's *t*-test and are indicated by *p*-values. N.S., no significance (*p*-value > 0.05).

701

702 Fig. S3 Time-lapse imaging of the QUEEN in *snf1*Δ *adk1*Δ cells

703 Time-lapse imaging of the QUEEN in *snf1*Δ *adk1*Δ cells in the 2% glucose medium. An
704 example of *snf1*Δ *adk1*Δ cell showing the irreversible drop of QUEEN ratio (indicated by an
705 arrowhead). In this case, the cell eventually died (indicated by an arrow). Images at the
706 representative time points were shown. The ATP concentration was plotted in the bottom.
707 White scale bar = 5 μm.

708

709 Fig. S4. Oscillatory behaviour of the ATP concentration visualized in the *bas1*Δ cell

710 (A) Another example of *bas1Δ* cells showing the oscillation of QUEEN ratio. In this case,
711 cytokinesis had just been completed at t = 0 min. ATP concentration of the cell-1 and the cell-2
712 were plotted in the bottom. See also movie S4. White scale bar = 5 μm. (B) Autocorrelation
713 function of the QUEEN ratio calculated from the data of cell-1 in Fig. 3E. Blue dotted lines
714 indicate 95% confidence interval. An arrow indicates the second peak of correlation that is
715 statistically significant and corresponds to the apparent period.

716

717 Fig. S5 *In silico* analysis of interactors of ATP mutants

718 Genetic and physical interactors of the indicated genes were derived from SGD database
719 (https://www.yeastgenome.org/) (Cherry et al., 2012) and overlaid on a functional map based

720 on the global genetic interaction network of the yeast genome (Baryshnikova, 2016, Usaj et al.,
721 2017). *URA6* encodes an uridylate kinase essential for viability, which also have adenylate
722 kinase activity.
723
724 Fig. S6 Simultaneous observation of Hsp104 and Pab1 foci
725 Wild-type cells expressing Hsp104-GFP and Pab1-RedStar2 were grown to log phase at 37°C
726 in the medium containing 2% glucose. The cells were washed and released either in the medium
727 containing 20 mM 2DG (top) or in the medium lacking glucose (bottom), and then imaged after
728 30 and 60 min. White scale bar = 5 μm.
729
730 Fig. S7 Cytotoxicity of polyQ containing Huntingtin protein in wild-type and
731 ATP-mutant yeast cells
732 Each strain of indicated genotype was transformed with an expression vector carrying Htt103Q
733 and grown on glucose ((-), no induction) or raffinose ((+), leaky expression) plates for 3 days at
734 30°C.
735

736 Table S1. *Strains used in this study*

Name	Genotype	Source	Figure
MTY3008	*snf1Δ::kanMX6 leu2Δ0 lys2Δ0 ura3Δ0*	Lab stock	4B, 6A-C, 6E, S7
MTY3015	*his3Δ1 leu2Δ0 lys2Δ0 ura3Δ0*	Lab stock	4B, 6A-E, S7
MTY3049	*adk1Δ::kanMX6 his3Δ1 leu2Δ0 lys2Δ0 ura3Δ0*	Lab stock	4B, 6A-E, S7
MTY3118	*bas1Δ::kanMX6 leu2Δ0 lys2Δ0 ura3Δ0*	Lab stock	4B, 6A-E, S7
MTY3143	*his3Δ1:: 2×pRS303-P_{TEF}-QUEEN-2m-T_{CYC1} leu2Δ0 lys2Δ0 ura3Δ0*	This study	S1
MTY3149	*adk1Δ::kanMX6 his3Δ1:: 2×pRS303-P_{TEF}-QUEEN-2m-T_{CYC1} leu2Δ0 lys2Δ0 ura3Δ0*	This study	S1
MTY3264	*his3Δ1:: 3×pRS303-P_{TEF}-QUEEN-2m-T_{CYC1} leu2Δ0 lys2Δ0 ura3Δ0 MYO1-3mCherry-hphMX6*	Takaine et al., 2019	2A-B, S2
MTY3270	*bas1Δ::kanMX6 his3Δ1:: 3×pRS303-P_{TEF}-QUEEN-2m-T_{CYC1} leu2Δ0 lys2Δ0 ura3Δ0 MYO1-3mCherry-hphMX6*	This study	2C-D, 3E, S2, S4
MTY3293	*adk1Δ::kanMX6 his3Δ1:: 3×pRS303-P_{TEF}-QUEEN-2m-T_{CYC1} leu2Δ0 lys2Δ0 ura3Δ0 MYO1-3mCherry-hphMX6*	This study	2A-B
MTY3355	*adk1Δ::kanMX6 snf1Δ::natNT2 his3Δ1:: 3×pRS303-P_{TEF}-QUEEN-2m-T_{CYC1} leu2Δ0 lys2Δ0 ura3Δ0 MYO1-3mCherry-hphMX6*	This study	2A-B, 3A-D, S3
MTY3371	*snf1Δ::kanMX6 his3Δ1:: 3×pRS303-P_{TEF}-QUEEN-2m-T_{CYC1} leu2Δ0 lys2Δ0 ura3Δ0 MYO1-3mCherry-hphMX6*	This study	2A-B, S2
MTY3412	*adk1Δ::kanMX6 snf1Δ::natNT2 leu2Δ0 lys2Δ0 ura3Δ0*	This study	4B, 6A-E, S7
MTY3420	*Hsp104-yeGFP-hphNT1 his3Δ1 leu2Δ0 lys2Δ0 ura3Δ0*	This study	4C-D, 5A-B
MTY3421	*snf1Δ::kanMX6 Hsp104-yeGFP-hphNT1 his3Δ1 leu2Δ0 lys2Δ0 ura3Δ0*	This study	4C-D
MTY3422	*bas1Δ::kanMX6 Hsp104-yeGFP-hphNT1 his3Δ1 leu2Δ0 lys2Δ0 ura3Δ0*	This study	4C-D
MTY3424	*adk1Δ::kanMX6 Hsp104-yeGFP-hphNT1 his3Δ1 leu2Δ0 lys2Δ0 ura3Δ0*	This study	4C-D
MTY3425	*adk1Δ::kanMX6 snf1Δ::natNT2 Hsp104-yeGFP-hphNT1 his3Δ1 leu2Δ0 lys2Δ0 ura3Δ0*	This study	4C-D
MTY3489	*atg1Δ::kanMX6 his3Δ1 leu2Δ0 lys2Δ0 ura3Δ0*	Lab stock	6E
MTY3493	*snq2Δ::KILeu2; pdr3Δ::KIura3; pdr1Δ::natMX4; can1Δ::STE2prSp_his5 lyp1Δ*	From Y.	Parental

	his3Δ1 leu2Δ0 ura3Δ0 met15Δ0 LYS2+	Ohya, (Piotrowski et al., 2017)	strain of MTY3501
MTY3501	*Hsp104-yeGFP-hphNT1 snq2Δ::KILeu2; pdr3Δ::KIura3; pdr1Δ::natMX4; can1Δ::STE2prSp_his5 lyp1Δ his3Δ1 leu2Δ0 ura3Δ0 met15Δ0 LYS2+*	This study	6F
MTY3503	*Pab1- yeGFP-hphNT1 his3Δ1 leu2Δ0 lys2Δ0 ura3Δ0*	This study	4D
MTY3504	*Hsp104-yeGFP-hphNT1 Pab1-RedStar2-natNT2 his3Δ1 leu2Δ0 lys2Δ0 ura3Δ0*	This study	S6
MTY3505	*snf1Δ::kanMX6 Pab1- yeGFP-hphNT1 his3Δ1 leu2Δ0 lys2Δ0 ura3Δ0*	This study	4D
MTY3506	*adk1Δ::kanMX6 Pab1- yeGFP-hphNT1 his3Δ1 leu2Δ0 lys2Δ0 ura3Δ0*	This study	4D
MTY3507	*adk1Δ::kanMX6 snf1Δ::natNT2 Pab1- yeGFP-hphNT1 his3Δ1 leu2Δ0 lys2Δ0 ura3Δ0*	This study	4D
MTY3508	*bas1Δ::kanMX6 Pab1- yeGFP-hphNT1 his3Δ1 leu2Δ0 lys2Δ0 ura3Δ0*	This study	4D
MTY3513	*atg1Δ::natNT2 adk1Δ::kanMX6 his3Δ1 leu2Δ0 lys2Δ0 ura3Δ0*	This study	6E
MTY3514	*atg1Δ::natNT2 snf1Δ::kanMX6 his3Δ1 leu2Δ0 lys2Δ0 ura3Δ0*	This study	6E
MTY3515	*atg1Δ::natNT2 bas1Δ::kanMX6 his3Δ1 leu2Δ0 lys2Δ0 ura3Δ0*	This study	6E
MTY3516	*rpn4Δ::natNT2 adk1Δ::kanMX6 his3Δ1 leu2Δ0 lys2Δ0 ura3Δ0*	This study	6E
MTY3517	*rpn4Δ::natNT2 snf1Δ::kanMX6 his3Δ1 leu2Δ0 lys2Δ0 ura3Δ0*	This study	6E
MTY3518	*rpn4Δ::natNT2 bas1Δ::kanMX6 his3Δ1 leu2Δ0 lys2Δ0 ura3Δ0*	This study	6E
MTY3525	*rpn4Δ::kanMX6 his3Δ1 leu2Δ0 lys2Δ0 ura3Δ0*	Lab stock	6A-C, 6E

738 Table S2. *Plasmids used in this study*

Name	Structure	Source	Purpose
MTP3091	pESC-Leu-GFP-Ubc9-ts	Judith Frydman (pJF1089)	Fig. 5C
MTP3088	p426 103Q GAL	Addgene (cat.# 1188)	Fig. S7
MTP3108	pYES2-α-synuclein-GFP	H. Takagi (Wijayanti et al., 2015)	Fig. 6A-D
MTP3090	pYES2-GFP	K. Ohashi	Fig. 6A

Captions for supplementary movies

Movie S1.

Time-lapse imaging of the QUEEN in *snf1*Δ*adk1*Δ cells in the 2% glucose medium. Corresponding to the data shown in Fig. 3A. The QUEEN ratio was dropped twice (116 min and 132 min) with short interval. White scale bar = 5 μm.

Movie S2.

Another example of *snf1*Δ*adk1*Δ cells showing the sudden drop of QUEEN ratio. Corresponding to the data shown in Fig. 3B. The QUEEN ratio was dropped twice (180 min and 356 min) with long interval. White scale bar = 5 μm.

Movie S3.

Oscillatory behavior of the QUEEN ratio in the *bas1*Δ cell. Corresponding to the data shown in Fig. 3E. Left, the QUEEN ratio image; middle, Myo1-mCherry (inverted grayscale image); right, bright field image. Images were taken every 4 min. White scale bar = 5 μm.

Movie S4.

Another example of *bas1*Δ cells showing the oscillation of QUEEN ratio. Corresponding to the data shown in Supplementary Fig. S4A. Left, the QUEEN ratio image; right, bright field image. In this case, cytokinesis had been already completed at t = 0 min. Images was taken every 3 min. White scale bar = 5 μm.

Fig. 1

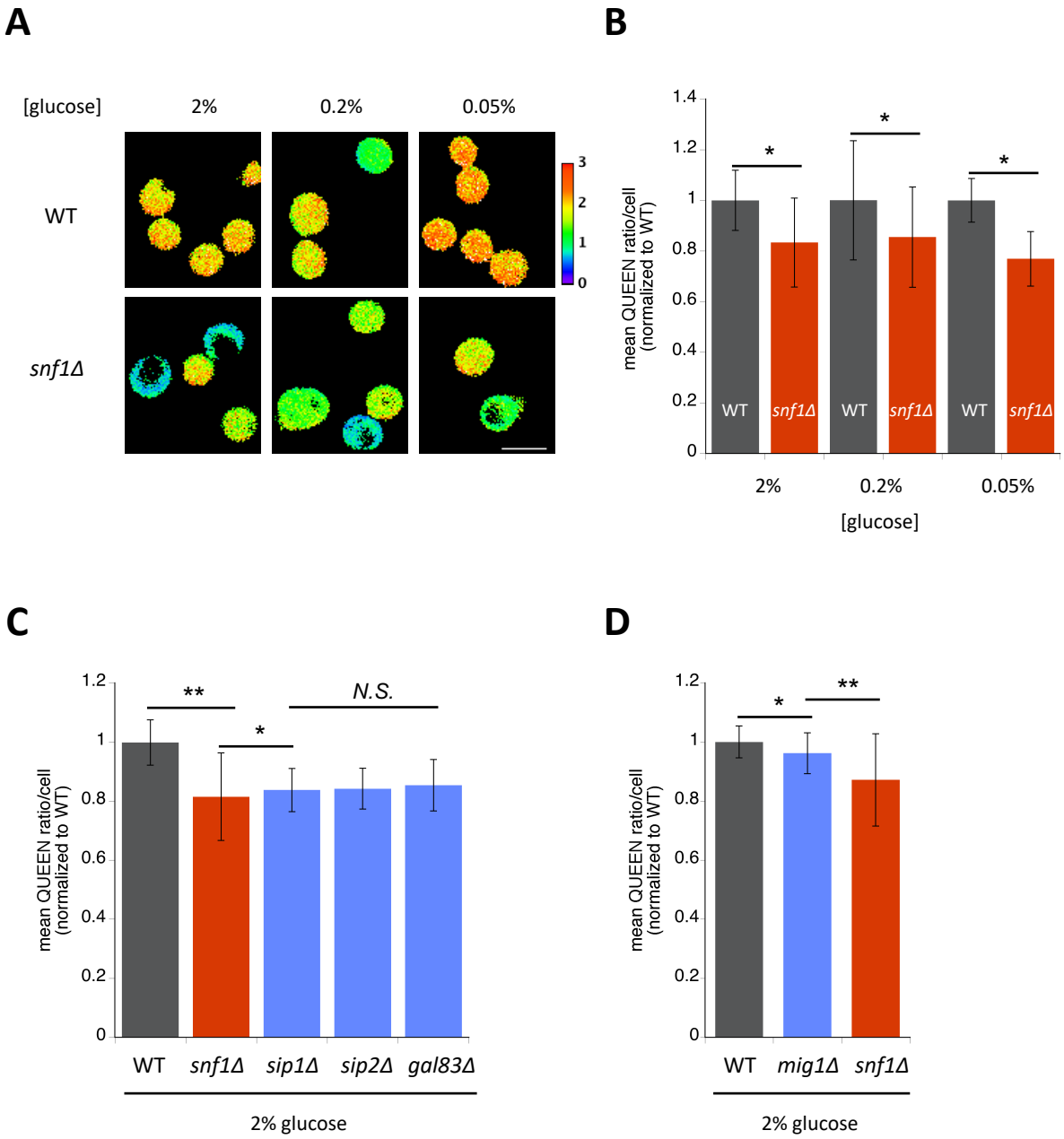
A
[glucose]
2%
0.2%
0.05%
WT
snf1Δ
3
2
1
0
B
mean QUEEN ratio/cell (normalized to WT)
1.4
1.2
1
0.8
0.6
0.4
0.2
0
*
*
*
WT
snf1Δ
WT
snf1Δ
WT
snf1Δ
2%
0.2%
0.05%
[glucose]
C
mean QUEEN ratio/cell (normalized to WT)
1.2
1
0.8
0.6
0.4
0.2
0
**
*
N.S.
WT
snf1Δ
sip1Δ
sip2Δ
gal83Δ
2% glucose
D
mean QUEEN ratio/cell (normalized to WT)
1.2
1
0.8
0.6
0.4
0.2
0
*
**
WT
mig1Δ
snf1Δ
2% glucose

Fig. 2

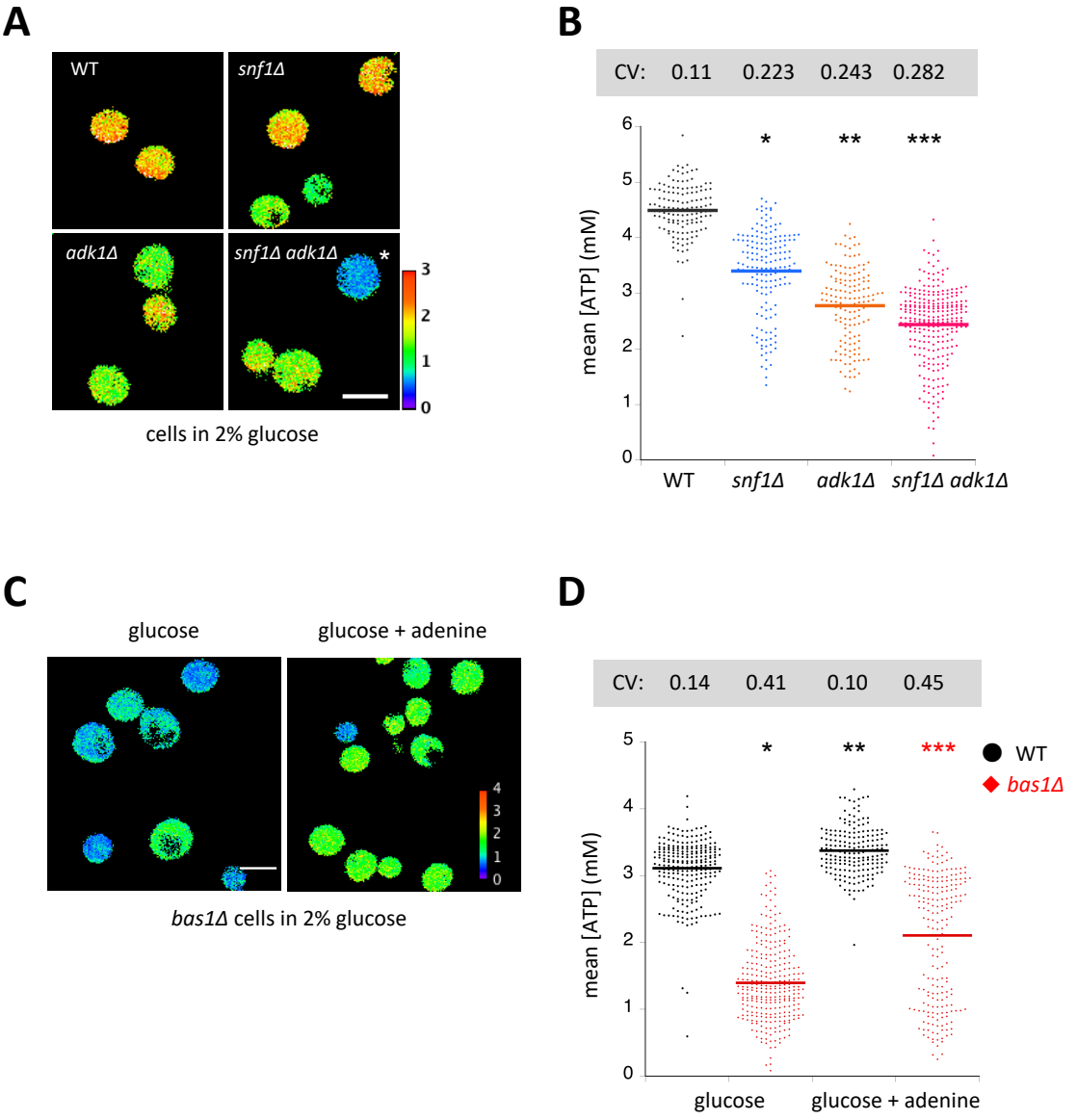
A
WT
snf1Δ
adk1Δ
snf1Δ adk1Δ
*
3
2
1
0
cells in 2% glucose
B
CV: 0.11 0.223 0.243 0.282
mean [ATP] (mM)
6
5
4
3
2
1
0
*
**
***
WT
snf1Δ
adk1Δ
snf1Δ adk1Δ
C
glucose
glucose + adenine
4
3
2
1
0
bas1Δ cells in 2% glucose
D
CV: 0.14 0.41 0.10 0.45
mean [ATP] (mM)
5
4
3
2
1
0
*
**
***
WT
bas1Δ
glucose
glucose + adenine

Fig. 3

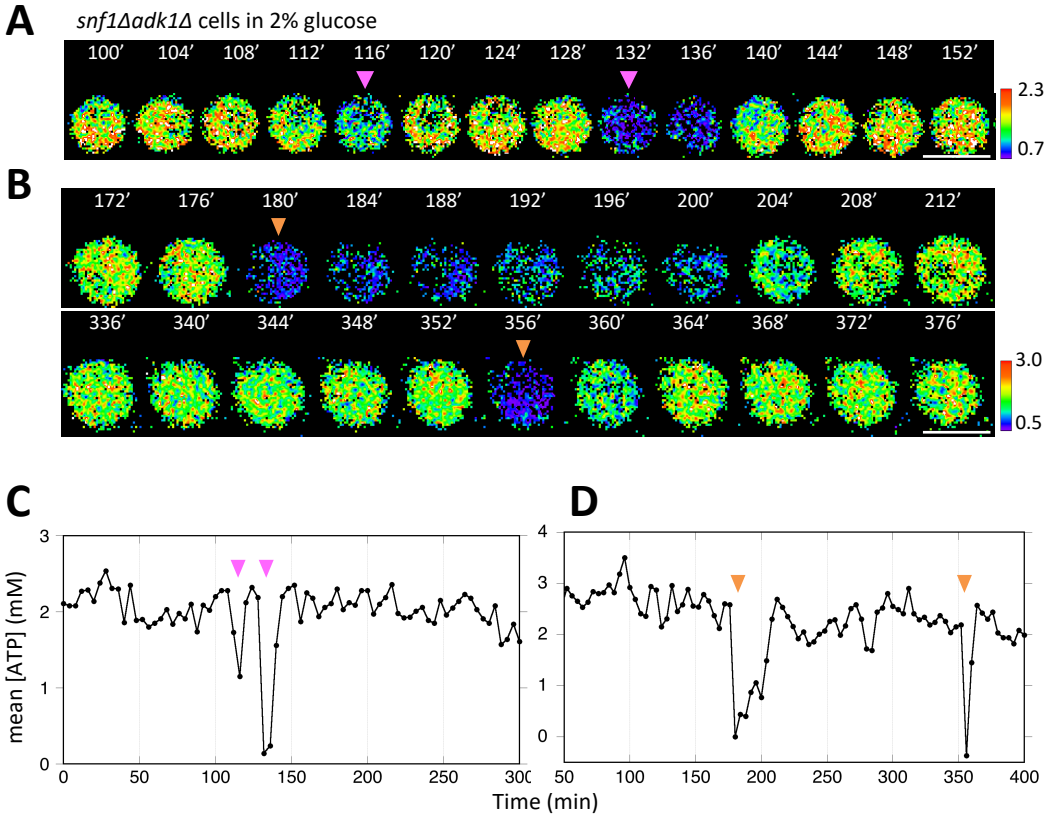
A
snf1Δadk1Δ cells in 2% glucose
100′ 104′ 108′ 112′ 116′ 120′ 124′ 128′ 132′ 136′ 140′ 144′ 148′ 152′
2.3
0.7
B
172′ 176′ 180′ 184′ 188′ 192′ 196′ 200′ 204′ 208′ 212′
336′ 340′ 344′ 348′ 352′ 356′ 360′ 364′ 368′ 372′ 376′
3.0
0.5
C
D
mean [ATP] (mM)
Time (min)

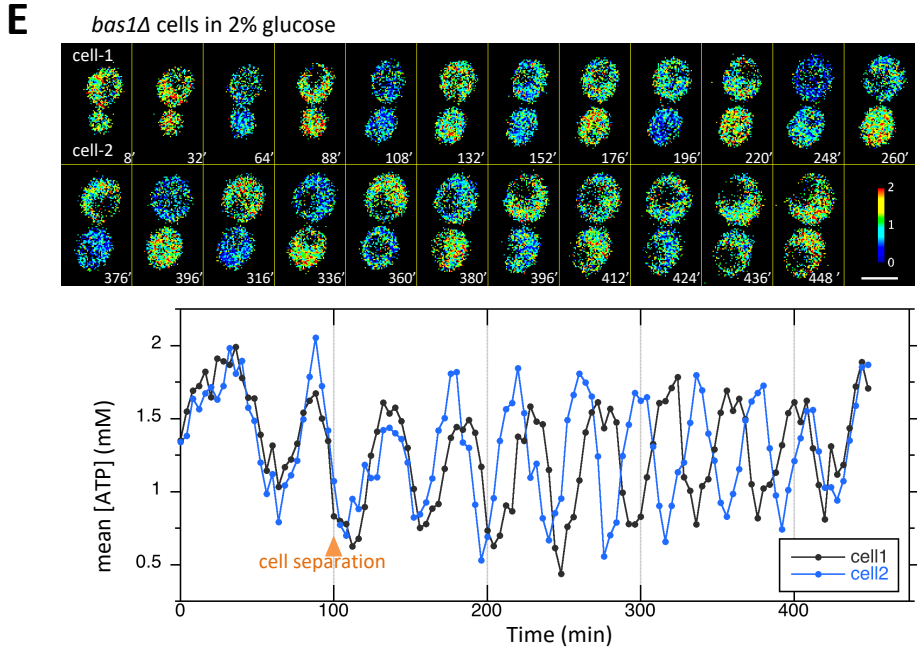
E
bas1Δ cells in 2% glucose
cell-1
cell-2
8′ 32′ 64′ 88′ 108′ 132′ 152′ 176′ 196′ 220′ 248′ 260′
376′ 396′ 316′ 336′ 360′ 380′ 396′ 412′ 424′ 436′ 448′
mean [ATP] (mM)
cell separation
cell1
cell2
Time (min)

Fig. 4

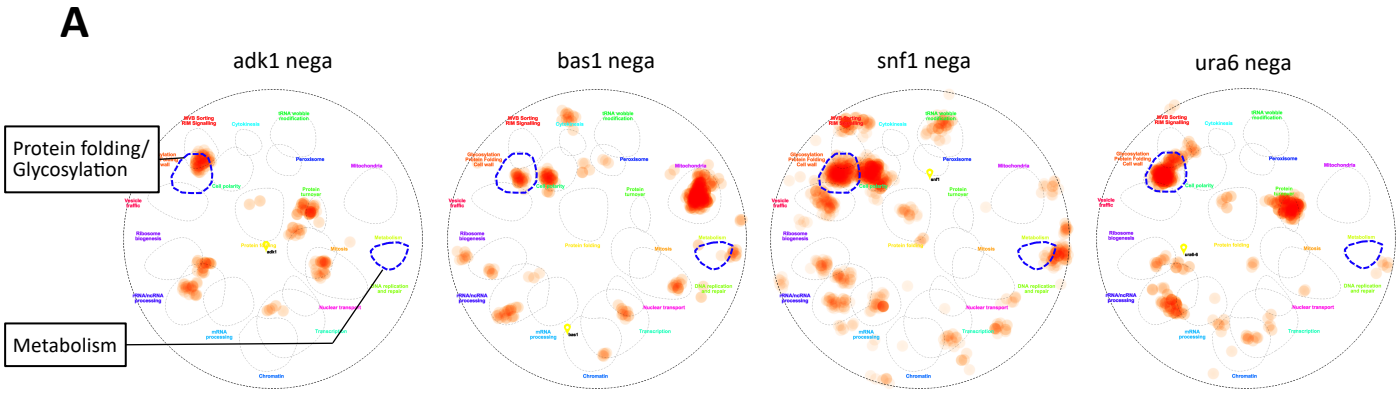
A
adk1 nega
bas1 nega
snf1 nega
ura6 nega
Protein folding/
Glycosylation
Metabolism

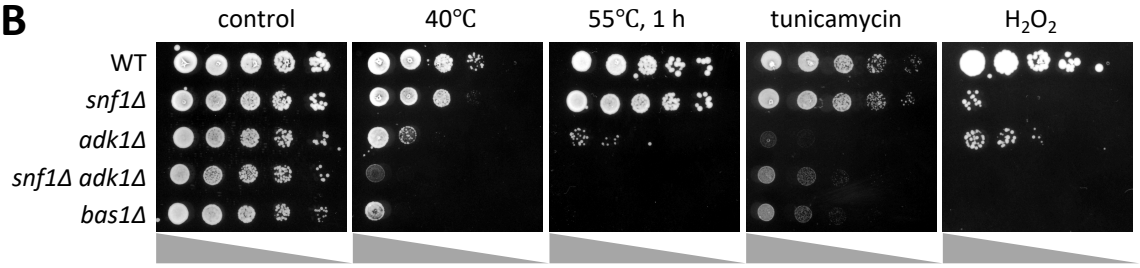
B
control
40°C
55°C, 1 h
tunicamycin
H_2O_2
WT
snf1Δ
adk1Δ
snf1Δ adk1Δ
bas1Δ

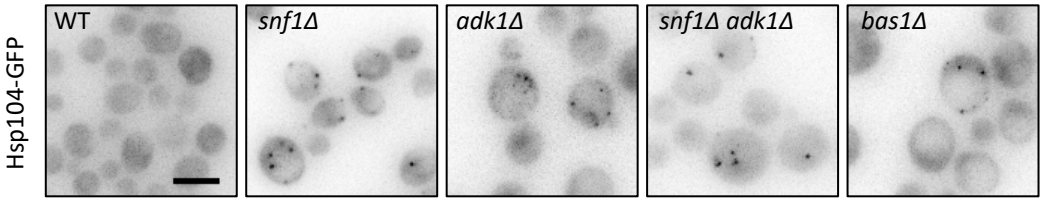
C
Hsp104-GFP
WT
snf1Δ
adk1Δ
snf1Δ adk1Δ
bas1Δ

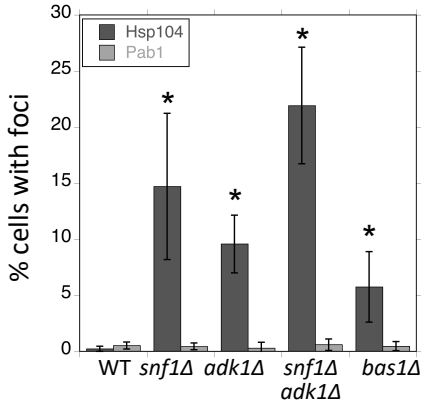
D
% cells with foci
Hsp104
Pab1
0
5
10
15
20
25
30
*
WT
snf1Δ
adk1Δ
snf1Δ adk1Δ
bas1Δ

Fig. 5

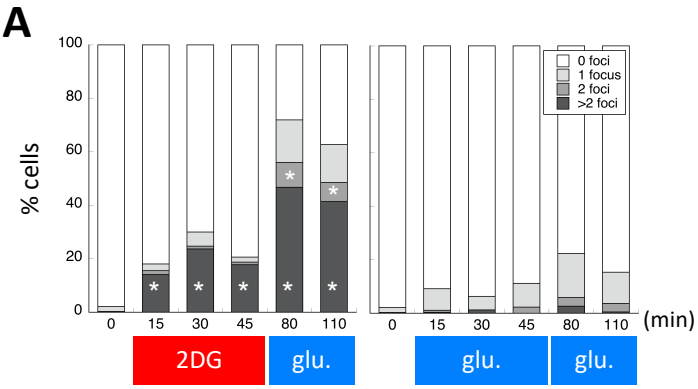
A
% cells
100
80
60
40
20
0
0 foci
1 focus
2 foci
>2 foci
0
15
30
45
80
110
(min)
2DG
glu.
glu.
glu.

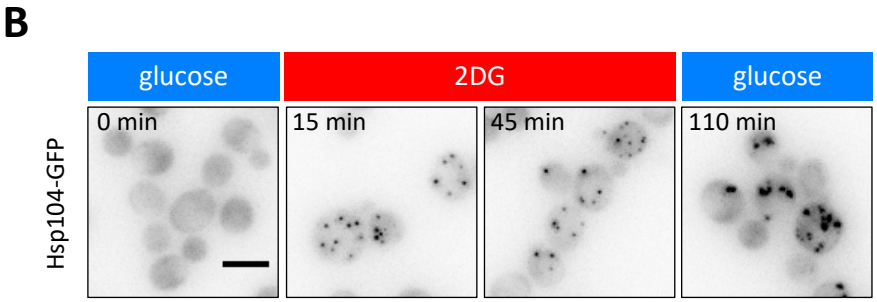
B
glucose
2DG
glucose
Hsp104-GFP
0 min
15 min
45 min
110 min

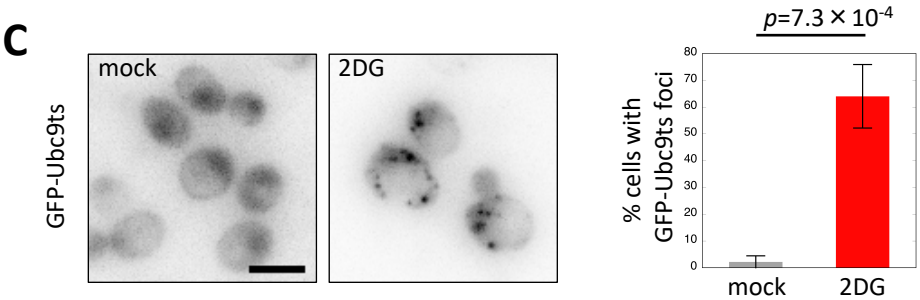
C
GFP-Ubc9ts
mock
2DG
p=7.3 × 10-4
% cells with GFP-Ubc9ts foci
80
70
60
50
40
30
20
10
0
mock
2DG

Fig. 6

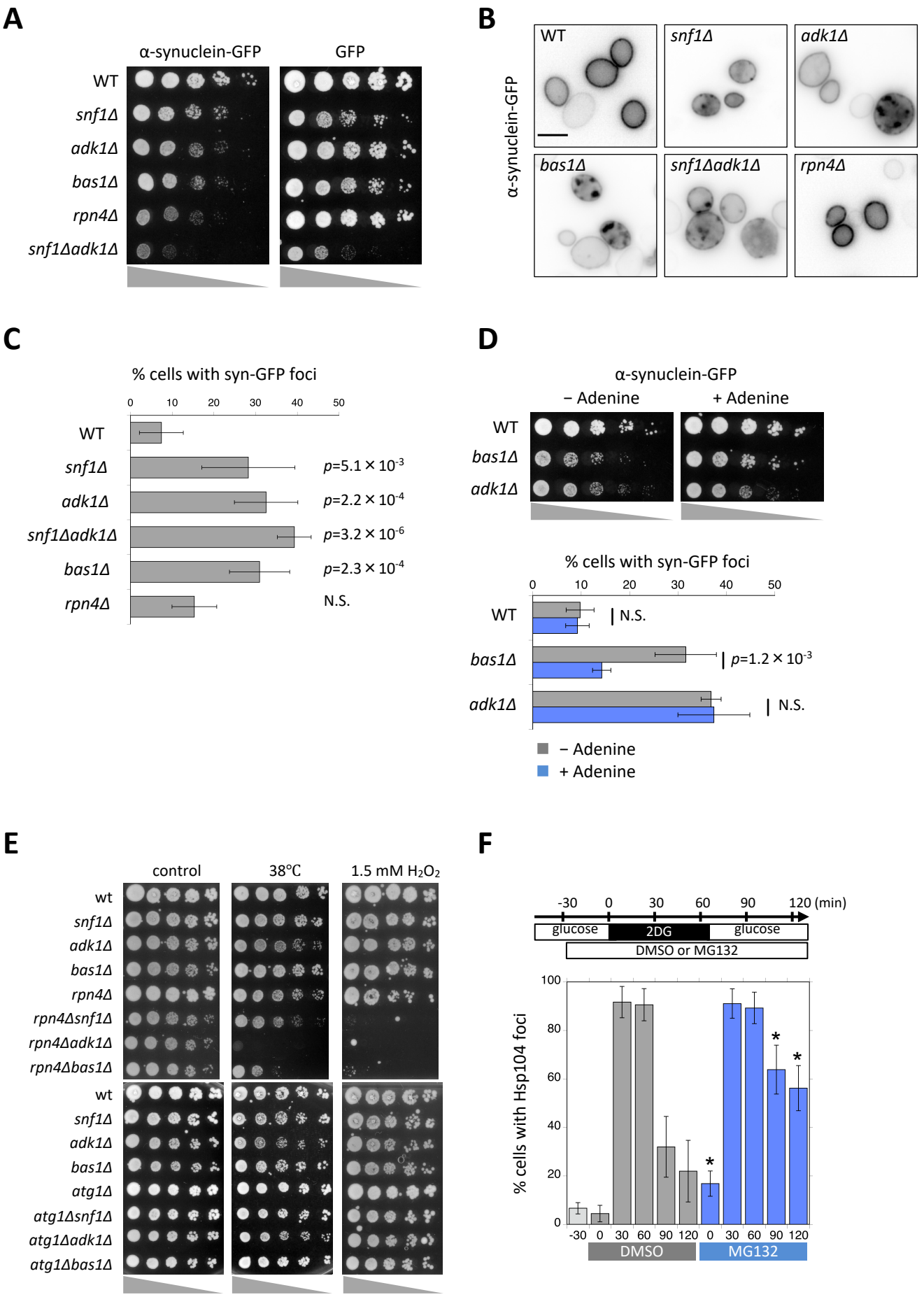
A
α-synuclein-GFP
GFP
WT
snf1Δ
adk1Δ
bas1Δ
rpn4Δ
snf1Δadk1Δ
B
α-synuclein-GFP
WT
snf1Δ
adk1Δ
bas1Δ
snf1Δadk1Δ
rpn4Δ
C
% cells with syn-GFP foci
0
10
20
30
40
50
WT
snf1Δ
adk1Δ
snf1Δadk1Δ
bas1Δ
rpn4Δ
p=5.1 × 10-3
p=2.2 × 10-4
p=3.2 × 10-6
p=2.3 × 10-4
N.S.
D
α-synuclein-GFP
− Adenine
+ Adenine
WT
bas1Δ
adk1Δ
% cells with syn-GFP foci
0
10
20
30
40
50
WT
N.S.
bas1Δ
p=1.2 × 10-3
adk1Δ
N.S.
− Adenine
+ Adenine
E
control
38°C
1.5 mM H2O2
wt
snf1Δ
adk1Δ
bas1Δ
rpn4Δ
rpn4Δsnf1Δ
rpn4Δadk1Δ
rpn4Δbas1Δ
wt
snf1Δ
adk1Δ
bas1Δ
atg1Δ
atg1Δsnf1Δ
atg1Δadk1Δ
atg1Δbas1Δ
F
-30
0
30
60
90
120 (min)
glucose
2DG
glucose
DMSO or MG132
% cells with Hsp104 foci
100
80
60
40
20
0
-30 0 30 60 90 120 0 30 60 90 120
DMSO
MG132

Fig. 7

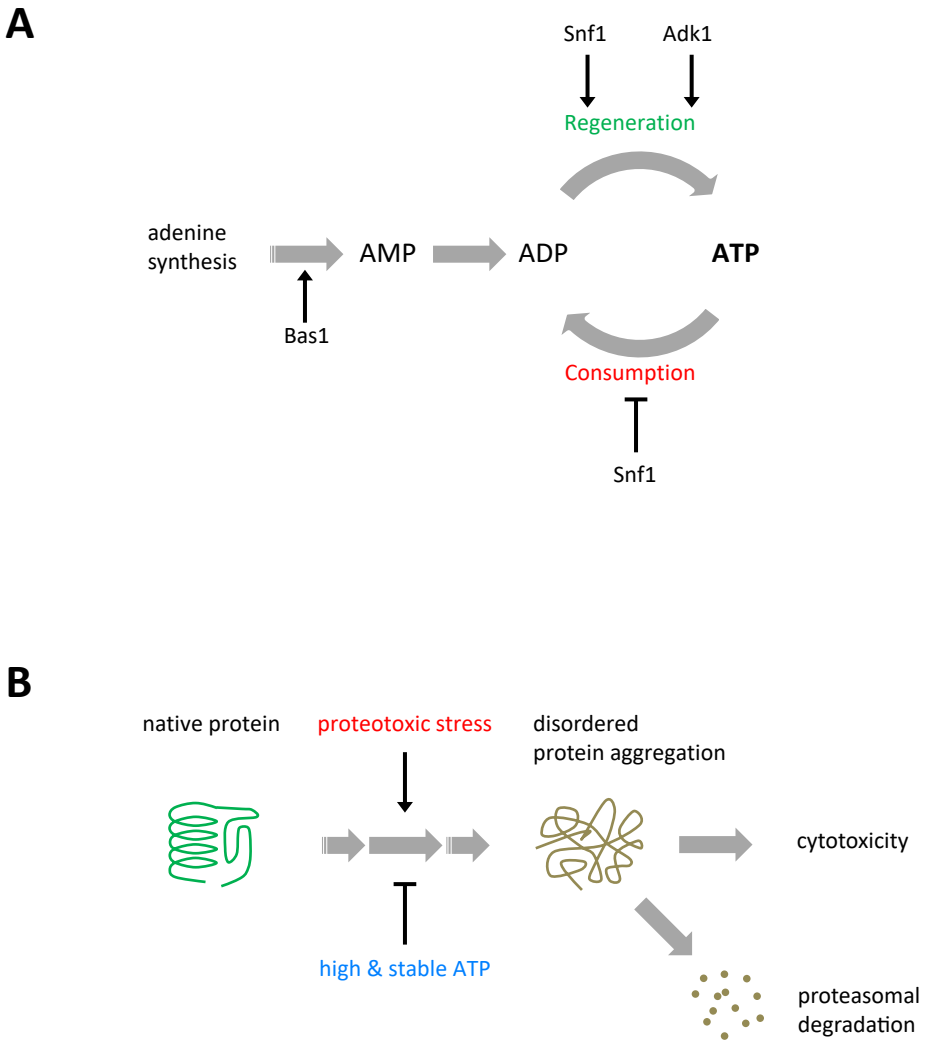
A
Snf1
Adk1
Regeneration
adenine
synthesis
AMP
ADP
ATP
Bas1
Consumption
Snf1
B
native protein
proteotoxic stress
disordered
protein aggregation
cytotoxicity
high & stable ATP
proteasomal
degradation

Fig. S1

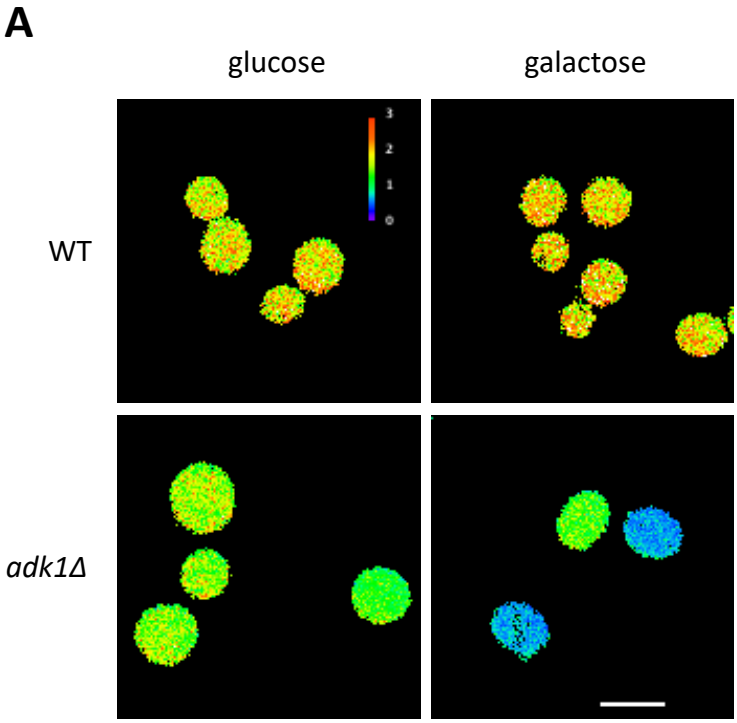
A
glucose
galactose
WT
adk1Δ
3
2
1
0

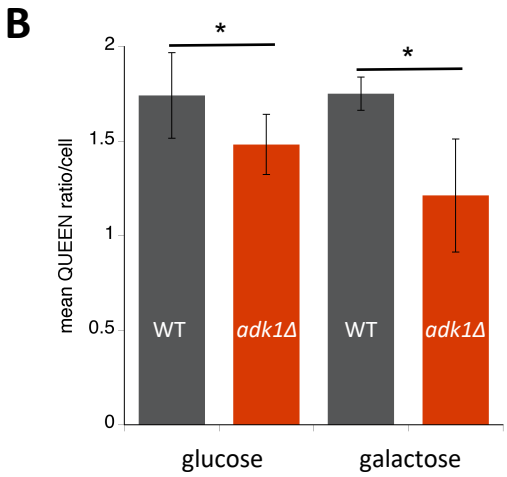
B
mean QUEEN ratio/cell
2
1.5
1
0.5
0
*
*
WT
adk1Δ
WT
adk1Δ
glucose
galactose

Fig. S2

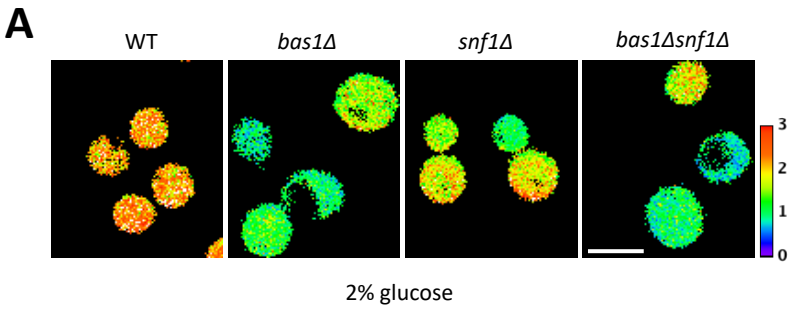
A
WT
bas1Δ
snf1Δ
bas1Δsnf1Δ
3
2
1
0
2% glucose

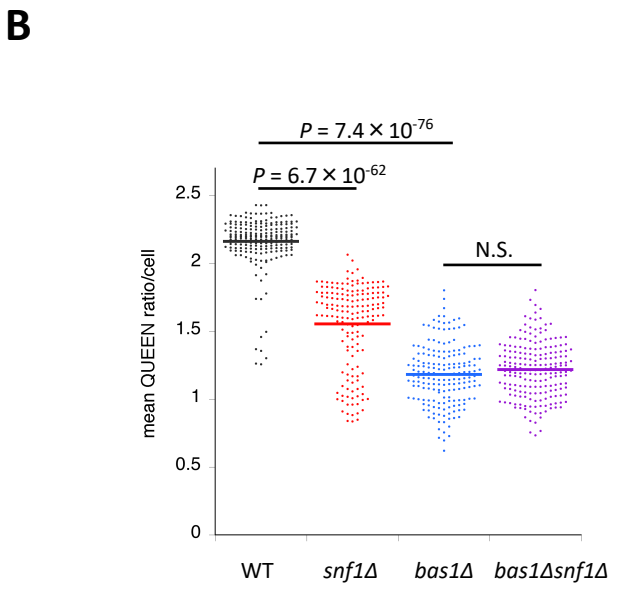
B
P = 7.4 × 10-76
P = 6.7 × 10-62
N.S.
mean QUEEN ratio/cell
2.5
2
1.5
1
0.5
0
WT
snf1Δ
bas1Δ
bas1Δsnf1Δ

Fig. S3

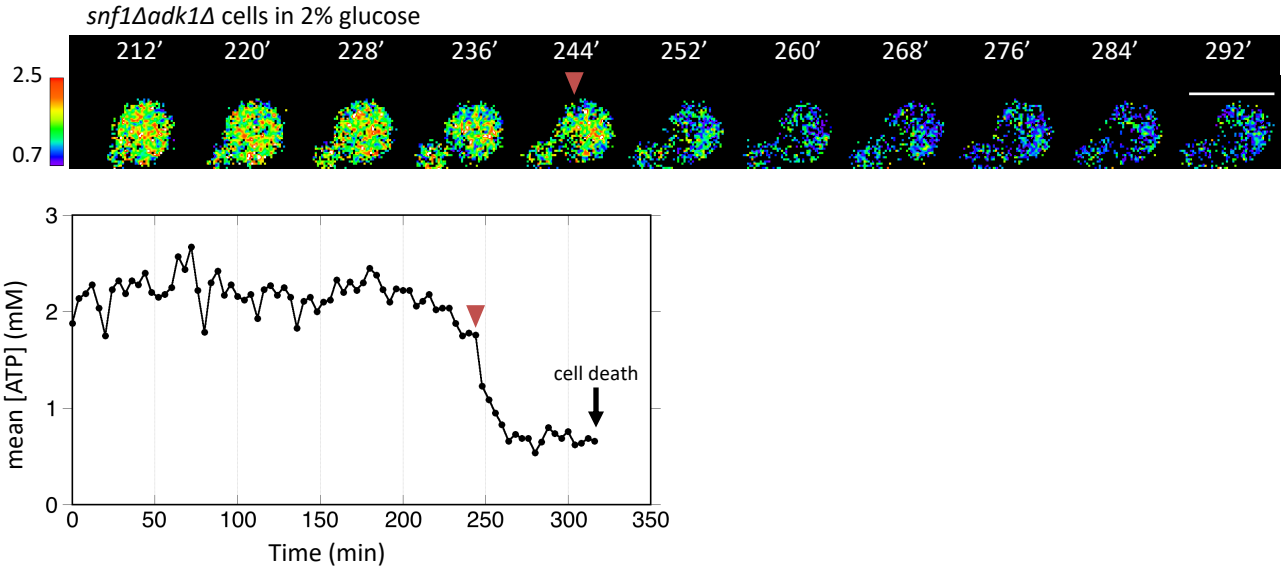
snf1Δadk1Δ cells in 2% glucose
212’
220’
228’
236’
244’
252’
260’
268’
276’
284’
292’
2.5
0.7
mean [ATP] (mM)
3
2
1
0
0
50
100
150
200
250
300
350
Time (min)
cell death

Fig. S4

A

bas1Δ cells in 2% glucose

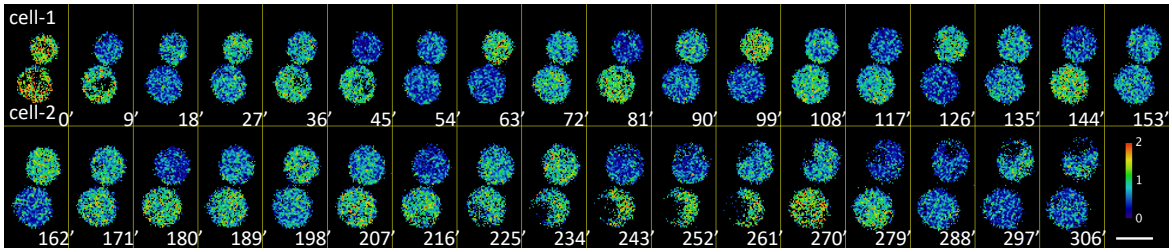

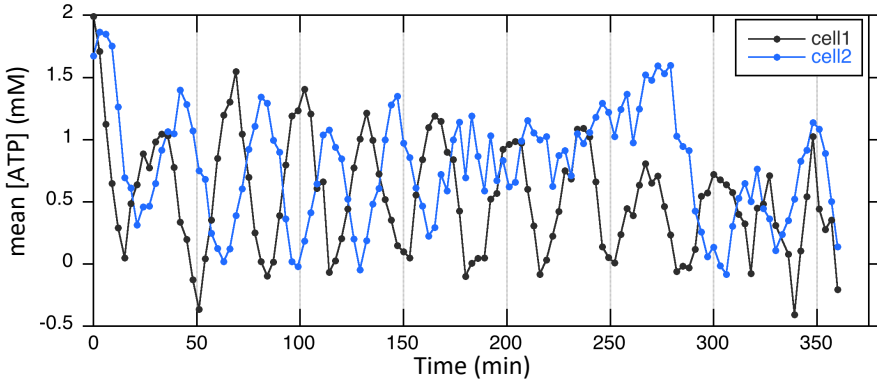

B

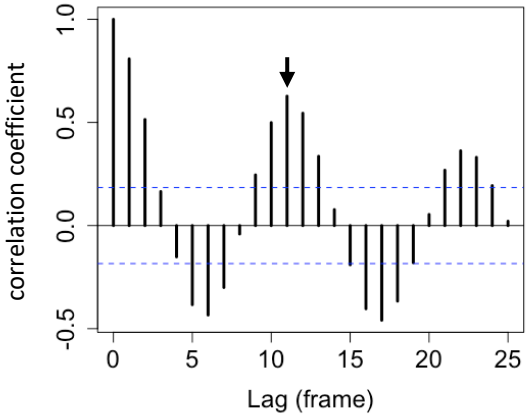

Fig. S5

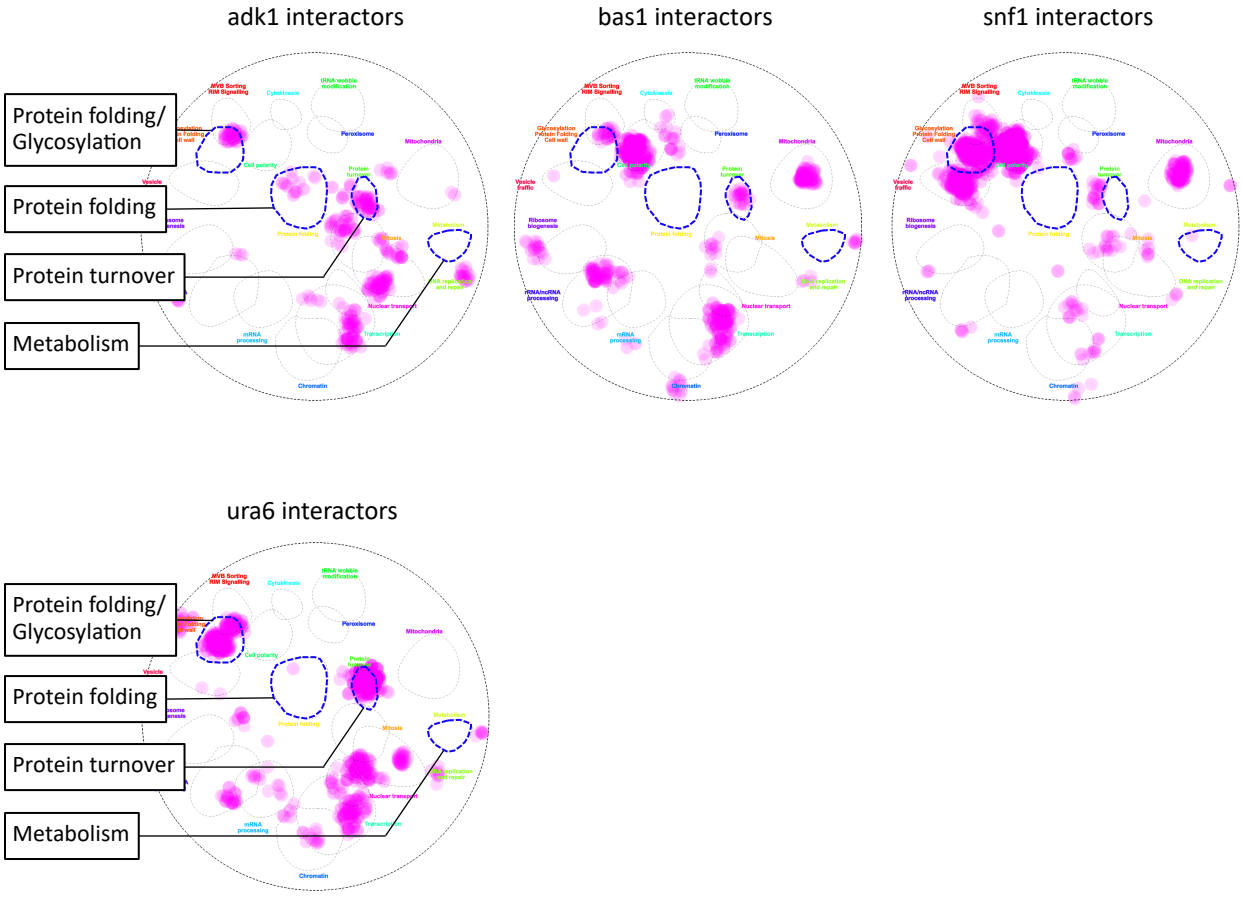
adk1 interactors
bas1 interactors
snf1 interactors
ura6 interactors
Protein folding/ Glycosylation
Protein folding
Protein turnover
Metabolism

Fig. S6

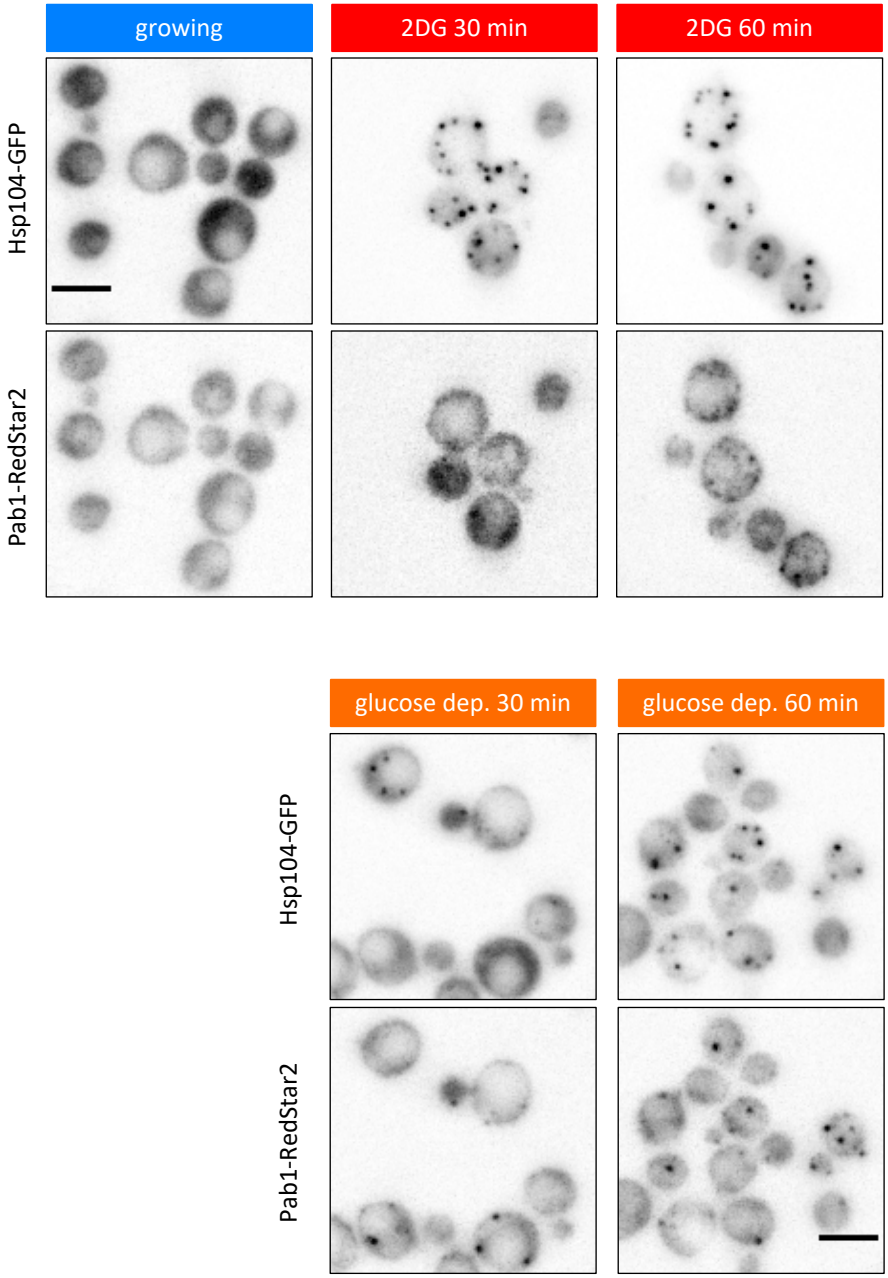
growing
2DG 30 min
2DG 60 min
Hsp104-GFP
Pab1-RedStar2
glucose dep. 30 min
glucose dep. 60 min
Hsp104-GFP
Pab1-RedStar2
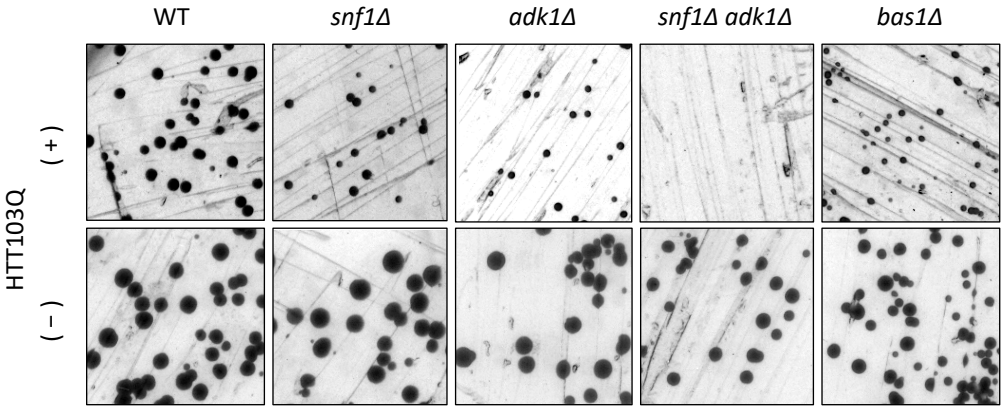
Fig. S7